2013/09/11
Head Id: 206028
Archive Id: 205902:206028M
Archive Date: 2013/09/06
Archive Tag: trunk

Measurement of the muon charge asymmetry in inclusive pp $\rightarrow$ W production at $\sqrt{s}$ =7 TeV

The CMS Collaboration

Abstract

We report on a measurement of the muon charge asymmetry in inclusive pp $\rightarrow$W+X production at $\sqrt{s}$=7 TeV. The data sample corresponds to an integrated luminosity of 4.7 fb^{-1} recorded by the CMS detector at the LHC. With a sample of more than 20 million W $\rightarrow \mu\nu$ events, the statistical precision is greatly improved in comparison to previous measurements. These new results provide additional constraints on the Parton Distribution Functions (PDFs) of the proton in the Björken parameter x range from 0.001 to 0.1.

1 Introduction

In pp collisions, W bosons are produced primarily via the processes $u\bar{d} \to W^+$ and $d\bar{u} \to W^-$. The quark in one of the protons is predominantly a valence quark which annihilates with a sea antiquark in the other proton. Because of the presence of two valence u quarks in the proton, there is an overall excess of W^+ over W^- bosons. The inclusive ratio of total cross sections for W^+ and W^- boson production at the Large Hadron Collider (LHC) has been measured to be $1.421 \pm 0.006(\text{stat.}) \pm 0.032(\text{syst.})$ by the Compact Muon Solenoid (CMS) experiment [1] and is in agreement with predictions of the Standard Model (SM) based on various parton distribution functions (PDFs) [2, 3]. Measurements of the production asymmetry between W^+ and W^- bosons as a function of boson rapidity provide additional constraints on the u/d ratio and on the sea antiquark densities in the proton. For pp collisions at $\sqrt{s} = 7$ TeV these measurements explore the parton distributions in the proton in Björken x from 0.001 to 0.1 [4]. However, it is difficult to measure the boson rapidity production asymmetry because of the energy carried away by neutrinos in leptonic W decays. A quantity more directly accessible experimentally is the lepton charge asymmetry, defined to be

$$\mathcal{A}(\eta) = \frac{\frac{d\sigma}{d\eta}(W^+ \to \ell^+\nu) - \frac{d\sigma}{d\eta}(W^- \to \ell^-\bar{\nu})}{\frac{d\sigma}{d\eta}(W^+ \to \ell^+\nu) + \frac{d\sigma}{d\eta}(W^- \to \ell^-\bar{\nu})},$$

where ℓ is the daughter charged lepton, η is the charged lepton pseudorapidity in the CMS lab frame ($\eta = -\ln[\tan(\frac{\theta}{2})]$ where θ is the polar angle), and $\frac{d\sigma}{d\eta}$ is the differential cross section for charged leptons from W boson decays.

High precision measurements of the W lepton asymmetry can improve our determination of PDFs. Both the W lepton charge asymmetry and the W production charge asymmetry were studied in $p\bar{p}$ collisions by the CDF and D0 experiments at the Fermilab Tevatron Collider [5, 6]. The ATLAS, CMS, and LHCb experiments also reported measurements of the lepton charge asymmetry using data collected during the 2010 LHC run [7–9]. Earlier measurements of the W lepton charge asymmetry extracted from CMS data used data samples of 840 pb^{-1} [10] and 234 pb^{-1} [11] for the electron and muon decay channels, respectively.

The impact of CMS measurements of the lepton charge asymmetry on PDF global fits were studied by several groups [12–14], which concluded that improvements on the uncertainties of PDFs for several quark flavors can be achieved with more precise data. In this paper, we report on an update of the muon charge asymmetry using a data sample with integrated luminosity of 4.7 fb^{-1} collected by the CMS detector at the LHC in 2011. The number of $W \to \mu\nu$ events (more than 20M) in this data sample is two orders of magnitude larger than the previous measurement [8]. The measurement reported here supersedes the previously reported preliminary result which was based on a fraction of the 2011 CMS data [11].

This paper is organized as follows. A brief description of the CMS detector is given in Section 2. The selection of $W \to \mu\nu$ candidates is described in Section 3. The corrections for residual charge-specific bias in the measurement of the muon transverse momentum (p_T) and in the muon trigger, reconstruction and selection efficiencies are discussed in Section 4. The extraction of the $W \to \mu\nu$ signal is described in detail in Section 5. Systematic uncertainties and the full correlation matrix are given in Section 6. The final results are presented in Section 7, followed by a summary and conclusion in Section 8.

2 CMS experiment

A detailed description of the CMS experiment is given in a previous communication [15]. The central feature of the CMS apparatus is a a superconducting solenoid 6 m in diameter and 13 m long which provides an axial field of 3.8 T. Within the field volume are the silicon pixel and strip tracker, the crystal electromagnetic calorimeter (ECAL) and the brass/scintillator hadron calorimeter (HCAL). Muons are measured in gas-ionization detectors embedded in the steel return yoke of the solenoid. The electromagnetic calorimeter consists of nearly 76 000 lead tungstate crystals which provide coverage in pseudorapidity $|\eta| < 1.479$ in the barrel region and $1.479 < |\eta| < 3.0$ in two endcap regions. A preshower detector consisting of two planes of silicon sensors interleaved with a total of 3 X_0 of lead is located in front of the ECAL endcaps. The ECAL has an ultimate energy resolution of better than 0.5% for unconverted photons with transverse energies above 100 GeV. Muons are measured in the pseudorapidity range $|\eta| < 2.4$, with detection planes constructed of drift tubes (DT), cathode strip chambers (CSC), and resistive plate chambers. Matching the muons to the tracks measured in the silicon tracker results in an η dependent p_T resolution of about 1-5% for muon p_T in the range 25-100 GeV.

CMS uses a right-handed coordinate system, with the origin at the nominal interaction point, the x-axis pointing towards the center of the LHC, the y-axis pointing up (perpendicular to the LHC plane), and the z-axis along the anticlockwise-beam direction. The polar angle, θ, is measured from the positive z-axis and the azimuthal angle, ϕ, is measured in the x-y plane.

3 Event reconstruction

The $W \to \mu\nu$ candidates are characterized by a high-p_T muon accompanied by missing transverse momentum ($\vec{\not{E}}_T$), due to the escaping neutrino. Experimentally, the $\vec{\not{E}}_T$ is determined as the negative vector sum of the transverse momenta of all particles reconstructed using a particle flow algorithm [16]. The $W \to \mu\nu$ candidates used in this analysis were collected using a set of isolated single-muon triggers with different p_T thresholds, which is the major difference from previous CMS measurements [8, 11]. The isolated muon trigger is necessary to help reduce the trigger rate while maintaining a relatively low muon p_T threshold. We use all the data-taking periods during which the isolated muon trigger is not pre-scaled. Other physics processes, such as multijet production (QCD background), Drell–Yan ($Z/\gamma^* \to \ell^+\ell^-$) production, $W \to \tau\nu$ production (EWK background), and top quark pair ($t\bar{t}$) production can produce high-p_T muons and mimic $W \to \mu\nu$ signal candidates. In addition, cosmic ray muons can mimic $W \to \mu\nu$ candidates.

Monte Carlo (MC) simulation is used to help evaluate the background contributions in the data sample. Primarily, next-to-leading order (NLO) MC simulations based on the POWHEG event generator [17] interfaced with the CT10 PDF model [3] are used. The τ in the $W \to \tau\nu$ decay process is simulated by the TAUOLA MC [18]. The QCD multijet background is generated with the PYTHIA event generator [19] interfaced with the CTEQ6L PDF model [20]. All generated events are passed through the CMS detector simulation using GEANT4 [21] and then processed using a reconstruction sequence identical to that used for data. Pile-up (PU) interactions are caused by additional low-multiplicity interactions which occur in the same or slightly different beam crossing as the "hard interaction" process such as W production. For the data used in this analysis, PU is significant, corresponding to an average of about 7 reconstructed primary interaction vertices for each beam crossing. The PU distribution in the MC simulation is generated with a different distribution from what is observed in the data. Therefore, the MC simulation is reweighted to match the distribution of the number of interactions per crossing

in the data.

The selection criteria for muon reconstruction and identification are described in detail in previous reports [22, 23]. Therefore, only a brief summary is given below. Muon candidates are reconstructed using two different algorithms: one starts with the inner silicon tracks and then requires a minimum number of matching hits in the muon chambers, and the other starts by finding tracks in the muon system and then matching them to silicon tracks. A global track fit including both the silicon track hits and muon chamber hits is performed to improve the quality of the reconstructed muon candidates. The p_{T} of the inner silicon track is used as the muon p_{T} and the charge is identified from the signed curvature of the silicon track. Cosmic ray contamination is reduced by requiring that the distance of closest approach to the leading primary vertex is small: $|d_{xy}| < 0.2$ cm. The remaining cosmic ray background yield is estimated to be about 10^{-5} of the expected $\mathrm{W} \to \mu\nu$ signal, and is therefore neglected [8]. The primary vertices in an event are ordered according to the scalar sum of the p_{T}^2 of associated charged tracks. The track-based muon isolation, Iso_{track}, is defined to be the scalar sum of transverse momentum of tracks in a cone of 0.3 (in η and ϕ) around the muon candidate. Muons are required to have $Iso_{track}/p_{\mathrm{T}} < 0.1$. Only muons within $|\eta| < 2.4$ are included in the data sample.

In every event, muons passing the above selection criteria are ordered according to p_{T}, and the leading muon is selected as the $\mathrm{W} \to \mu\nu$ candidate. In each event the muon is required to be the particle that triggered the event. In addition, the muon is required to have $p_{\mathrm{T}} > 25\,\mathrm{GeV}$, which is the lowest momentum safely above the trigger turn-on threshold. Events which have a second muon with $p_{\mathrm{T}} > 15\,\mathrm{GeV}$ are rejected to reduce the background from Drell-Yan dimuon events ("Drell-Yan veto"). Note that the muon p_{T} is corrected for bias in the measurement of the momentum (discussed below) prior to the application of the $p_{\mathrm{T}} > 25\,\mathrm{GeV}$ selection cut. The rejected events, predominantly $\mathrm{Z}/\gamma^* \to \mu^+\mu^-$ events, are also used as a Drell-Yan control sample to study the modeling of the missing transverse energy ($\not\!\!E_{\mathrm{T}}$) in data and also provides constraints on the modeling of the transverse momentum spectrum of W and Z bosons. In addition, the sample is used to set the level of the background from Drell-Yan events for which the second muon is not identified.

The $\mathrm{W} \to \mu\nu$ candidates which pass the above selection criteria are divided into 11 bins in absolute value of muon pseudorapidity ($|\eta|$):

[0.0, 0.2], [0.2, 0.4], [0.4, 0.6], [0.6, 0.8], [0.8, 1.0], [1.0, 1.2], [1.2, 1.4], [1.4, 1.6], [1.6, 1.85], [1.85, 2.1], and [2.1, 2.4].

The muon charge asymmetry is measured in each of the $|\eta|$ bins, along with the determination of the correlation matrix of the systematic errors between different $|\eta|$ bins.

4 Muon momentum correction and efficiency studies

After the alignment of the tracker detector, a residual misalignment remains which is not perfectly reproduced in the MC simulation. The misalignment leads to a charge-dependent bias in the reconstruction of muon momenta. This bias is removed by using a muon momentum correction. The detailed description of the method for the extraction of the correction factors using $\mathrm{Z}/\gamma^* \to \mu^+\mu^-$ events is given in reference [24]. Here we only provide a short summary of the method. First, corrections to muon momentum in bins of η and ϕ are extracted separately for positive and negative muons using the average of the $1/p_T$ spectra of muons in $\mathrm{Z}/\gamma^* \to \mu^+\mu^-$ events. The $1/p_T$ spectra at the MC generator-level smeared by the reconstruction resolution are used as "Reference". The means of reconstructed spectra in data or MC simulation are

tuned to match the "Reference". Second, the correction factors derived in the previous step are tuned by comparing the dimuon invariant mass in each bin of muon charge Q and η to the "Reference". By comparing the correction factors for positively and negatively charged muons in each bin we can determine the relative contributions of bias from misalignment and from uncertainties of the magnetic field in the tracker system. We find that the bias is predominantly from misalignment. The same procedure is preformed for both data and reconstructed MC events, and correction factors are determined separately.

The average of the Z mass (mass profile) as a function of muon Q and η prior and posterior to the $1/p_T$ tuning is shown in Figure 1. The Z mass profiles posterior to the correction are compared to the reference mass profile for data and MC respectively. They agree well with the reference and the muon scale bias is largely removed. Note that the reference mass profile is expected to be a function of η because of the p_T cuts on the two daughter muons. The correction factors are extracted using the same η binning defined above in order to avoid correlations between different η bins.

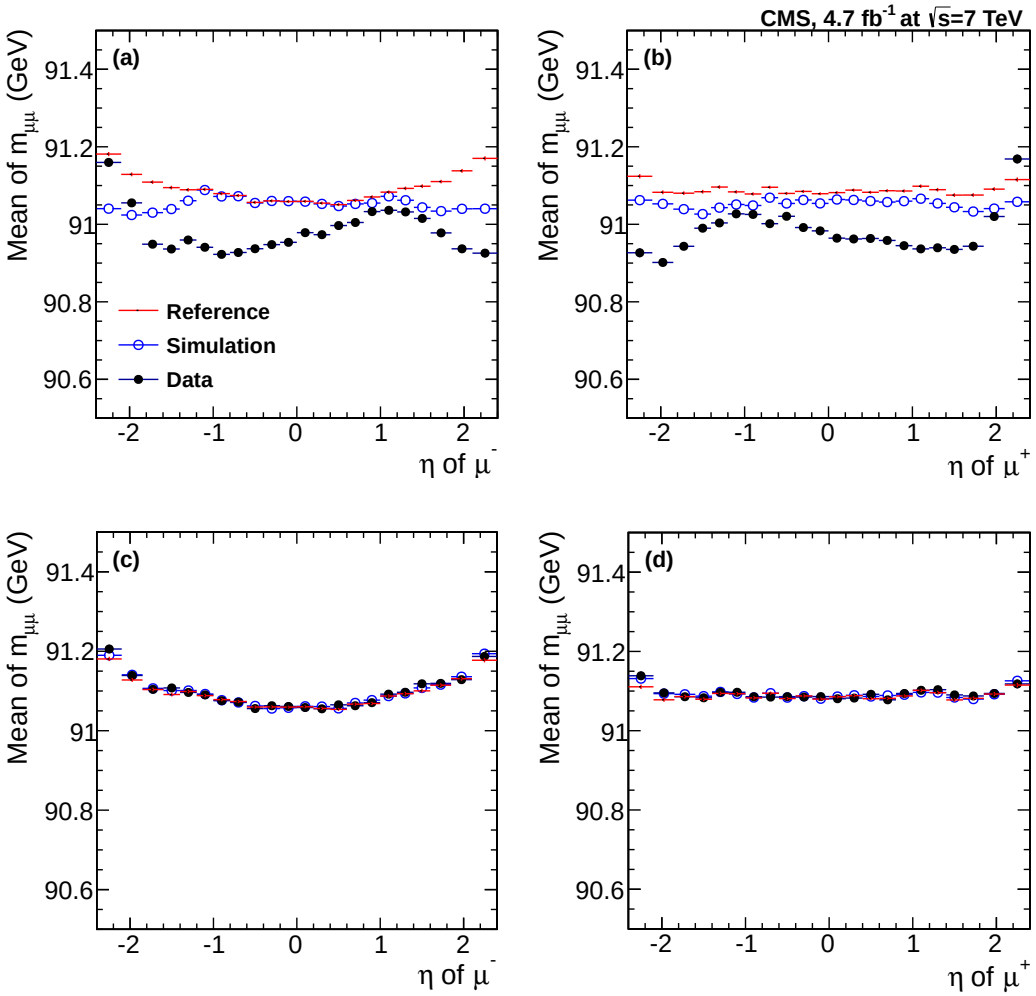

Figure 1: The Z mass profile as a function of muon η for μ^- (a, c) and μ^+ (b, d), where (a) and (b) are prior the correction and (c) and (d) are posterior the correction.

The overall efficiency in the selection of muon candidates includes contributions from recon-

struction, identification (including isolation), and trigger efficiencies. The muon reconstruction efficiency includes contributions from the reconstruction efficiency in the inner tracker system ("tracking") and in the outer muon system. The muon "offline" efficiency is the product of reconstruction and identification efficiencies. The contribution of each component to the overall efficiency (tracking, outer muon reconstruction, identification, and trigger) is measured directly from the $Z/\gamma^* \to \mu^+\mu^-$ events using the Tag-and-Probe method [22]. In the Tag-and-Probe method one of the daughter muons is used to tag the $Z/\gamma^* \to \mu^+\mu^-$ event and another muon candidate is used as a probe to study the muon efficiencies as a function of Q, η, and p_T. For every event a positively charged muon can be selected as the tag and a negatively charged probe candidate is used to study the efficiencies of negatively charged muons. The same procedure is repeated by selecting a negatively charged muon as the tag to study efficiencies of positively charged muons. Each individual efficiency is determined in 22 bins of muon η as defined above and 7 bins of p_T ([15, 20, 25, 30, 35, 40, 45, infinite]) for μ^+ and μ^-, respectively. The same procedure is done for both data and MC simulation and scale factors are determined to match the efficiencies in MC to the data.

The measured average tracking efficiency in each η bin varies from 99.6 to 99.9% with a slight inefficiency in transition regions from the barrel segments to the endcap segments and at the edge of the tracker system. The ratio of tracking efficiency between μ^+ and μ^- is consistent with 1.0 within statistical uncertainty. In the transition regions from the DT to the CSC, there is evidence that the muon offline efficiency has a slight asymmetry between μ^+ and μ^-. The ratio of efficiencies for positive and negative muon differs from 1.0 by up to 1.0±0.3%. The trigger efficiency ratio is also found to differ from 1.0 in some η regions. The maximum deviation is at η >2.1 where efficiency for μ^+ is about 2.0±0.5% higher than for μ^-. Figure 2 shows the pseudorapidity distribution for the leading μ^+ and μ^- in the $Z/\gamma^* \to \mu^+\mu^-$ sample. Here the MC simulation is corrected for muon momentum bias, efficiency and mis-modeling of the underlying physics before normalizing to yields in data. The pseudorapidity dependence of data and MC are in very good agreement.

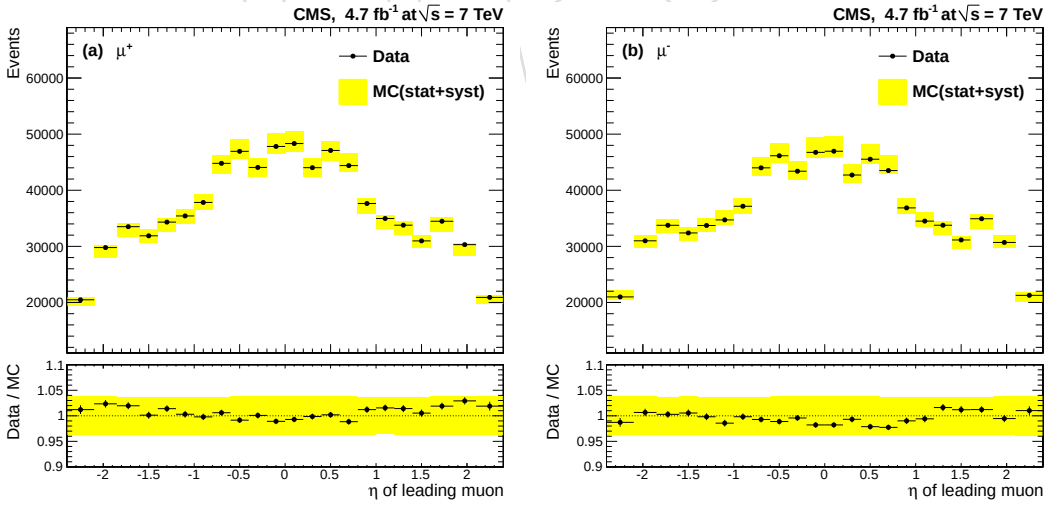

Figure 2: Pseudorapidity distribution of the leading μ^+ (a) and the μ^- (b) in $Z/\gamma^* \to \mu^+\mu^-$ sample. The dimuon invariant mass is within $60 < m_{\mu\mu} < 120$ GeV. The MC simulation is normalized to data yields. The yellow band is the total uncertainty in predicting the $Z/\gamma^* \to \mu^+\mu^-$ event yields using MC simulation, as described in Section 6.

5 Extraction of the signal for W events

After the event selection described above, there are a total of 12.9 million $W^+ \to \mu^+\nu$ and 9.1 million $W^- \to \mu^-\bar{\nu}$ candidate events. The expected backgrounds from QCD, EWK and $t\bar{t}$ events in the $W \to \mu\nu$ data sample are about 8%, 8%, and 0.5%, respectively. The background composition can vary for different $|\eta|$ bins. The background from single top-quark and diboson WW/WZ/ZZ production is less than 0.1%.

Binned maximum likelihood fits of the $\not\!\!E_T$ distributions are simultaneously performed for W^+ and W^- candidate events to extract the W^+ yield (N^{W^+}) and the W^- yield (N^{W^-}) for each $|\eta|$ bin. The likelihood is constructed following the Barlow-Beeston method to take into account the finite Monte Carlo statistics [25]. The $W \to \mu\nu$ MC sample is about the same size as the $W \to \mu\nu$ candidates in data. To avoid the large spread of weights introduced by PU reweighting, each MC sample is matched to the data PU distribution using an "accept-reject" technique based on the data/MC PU distributions.

The shapes of the $\not\!\!E_T$ distributions for the $W \to \mu\nu$ signal and background contributions are taken directly from MC simulations after correcting for mis-modeling of detector response and underlying physics. The normalizations of N^{W^+}, N^{W^-}, and QCD backgrounds are allowed to float. The ratio of the QCD backgrounds for W^+ and W^- candidate events is fixed using a QCD-enriched data control sample, which was collected using a non-isolated muon trigger. The Drell-Yan production cross section is rescaled using the yields in the Drell-Yan control sample, and the expected Drell-Yan background is normalized using this rescaled normalization factor. The $W \to \tau\nu$ background is normalized to the $W \to \mu\nu$ yield in data and the ratio of $W \to \tau\nu$ to $W \to \mu\nu$ is determined from MC simulation. The $t\bar{t}$ background is normalized to the QCD-NLO cross sections obtained from MCFM [26]. Note that the efficiency in the MC is scaled to match the efficiency in the data before the extraction of the background normalization factors.

The observed raw charge asymmetry ($\mathcal{A}^{raw}$) is related to the N^{W^+} and N^{W^-} by the following equation,

$$\mathcal{A}^{raw} = \frac{N^{W^+} - N^{W^-}}{N^{W^+} + N^{W^-}}. \quad (1)$$

Fixing the ratio of QCD background between W^+ and W^- candidate events introduces a correlation between the uncertainties in N^{W^+} and N^{W^-}. This is taken into account when evaluating the uncertainty of the raw charge asymmetry ($\mathcal{A}^{raw}$).

The simulation of the $\not\!\!E_T$ distribution in the CMS $Z/\gamma^* \to \mu^+\mu^-$ MC samples is not in perfect agreement with what is observed in data. A Φ-modulation of the $\vec{\not\!\!E}_T$ distribution is observed in both data and MC simulation, where the phase and amplitude of the modulation is different between data and simulation. Different sources, such as PU, mis-alignment within sub-detectors or between different sub-systems, and mis-modeling of detector response in simulation, can contribute to differences in the $\not\!\!E_T$ distributions for data and MC. In this analysis, the PU distribution in the MC simulation is reweighted to match the number of events per crossing seen in the data. In addition, $\vec{\not\!\!E}_T$ is corrected for the muon momentum scale bias as described in Section 4. This is done by adding the muon p_T scale correction vectorially to the $\vec{\not\!\!E}_T$ in data and MC simulation, respectively. However, a disagreement remains at a significant level which can potentially result in large systematic uncertainty in the measured charge asymmetry. Therefore, the $Z/\gamma^* \to \mu^+\mu^-$ control sample is used to empirically parametrize the mis-modeling to improve data-MC agreement. We use the "hadronic-recoil" technique (which has been previously used in both Tevatron experiments and in CMS [27–29]), as described below.

5.1 Definition of the "hadronic recoil"

The "hadronic recoil", $\vec{u}$, is defined as a vector sum of transverse momenta of all particle candidates excluding the candidate muon(s). In W $\to \mu\nu$ events, it is related to the $\vec{\not{E}}_{\mathrm{T}}$ as follows,

$$\vec{u} = -\vec{\not{E}}_{\mathrm{T}} - \vec{p_{\mathrm{T}}}, \tag{2}$$

where $\vec{p_{\mathrm{T}}}$ is the muon transverse momentum. In $\mathrm{Z}/\gamma^* \to \mu^+\mu^-$ events, it is defined to be

$$\vec{u} = -\vec{\not{E}}_{\mathrm{T}} - \vec{q}_T \tag{3}$$

where $\vec{q}_T$ is the transverse momentum of the di-muon system.

In the $\mathrm{Z}/\gamma^* \to \mu^+\mu^-$ event sample, the parallel and perpendicular component of $\vec{u}$ relative to boson $\vec{q}_T$ are defined as $u_{||}$and $u_\perp$respectively. The mean of $u_\perp$, $\tilde{u}_\perp$, is about 0. The mean of $u_{||}$, average recoil $\tilde{u}_{||}$, is close to the mean of the boson q_T, which is the detector response to the hadronic activity recoiling against the boson transverse momentum. The data-MC difference of the hadronic recoil distributions seen in the $\mathrm{Z}/\gamma^* \to \mu^+\mu^-$ sample is used to improve the the modeling of the $\not{E}_{\mathrm{T}}$ in the MC for W events and other physics processes. The procedure of extracting empirical corrections from the $\mathrm{Z}/\gamma^* \to \mu^+\mu^-$ sample and applying them to other physics processes is described below.

5.2 Correction procedure

The first step in the procedure is to correct the $\vec{\not{E}}_{\mathrm{T}}$ for both the muon scale bias described in Section 4, and the Φ-modulation described above. The Φ-modulation of $\vec{\not{E}}_{\mathrm{T}}$ is largely due to the fact that collisions, including hard-interactions that produce W events as well as PU events do not occur exactly at the origin of the CMS lab frame. This modulation can be characterized by a cosine function, $C \cdot \cos(\Phi - \Phi_0)$. The dependence of the amplitude C and phase term Φ_0 on the number of offline primary vertices (n) is extracted from the $\mathrm{Z}/\gamma^* \to \mu^+\mu^-$ event sample. This is done by fitting the Φ-dependent $(u_{||} - \tilde{u}_{||})(q_T)$ profile. Here the $\tilde{u}_{||}(q_T)$ can be parametrized by

$$-\tilde{u}_{||}(q_T) = (c_0 + c_1 q_T)\left(1 + erf(\alpha q_T^{\beta})\right), \tag{4}$$

where c_0, c_1, α, and β are floating parameters and $erf(x)$ is the error function. The amplitude C is found to depend linearly on the number of primary vertices n, while the Φ_0 is almost independent of PU. The measured C and Φ_0 distributions are different between the $\mathrm{Z}/\gamma^* \to \mu^+\mu^-$ data sample and the corresponding MC simulation. The Φ-modulation of $\vec{\not{E}}_{\mathrm{T}}$ can be removed by adding a 2-D vector ($C\cos(\Phi_0)$, $C\sin(\Phi_0)$) to the $\vec{\not{E}}_{\mathrm{T}}$ distribution, with C and Φ_0 extracted from $\mathrm{Z}/\gamma^* \to \mu^+\mu^-$ events.

The second step is to determine the hadronic recoil in $\mathrm{Z}/\gamma^* \to \mu^+\mu^-$ events. The $\tilde{u}_{||}(q_T)$ is measured as a function of boson q_T in 4 bins of leading jet $|\eta_j|$: [0.0, 1.2], [1.2, 2.4], [2.4, 3.0], and [3.0, 5.0]. The jets are formed by clustering particle flow candidates using anti-k_T jet clustering algorithm with cone size 0.5 [30]. The identified muon candidates are removed prior to the jet reconstruction. In each $|\eta_j|$ bin, the q_T-dependence of $\tilde{u}_{||}(q_T)$ is parametrized by Eq. 4. The resolutions of $u_{||}$and $u_\perp$in each boson q_T are determined by fitting a Gaussian function to the $u_{||} - \tilde{u}_{||}$ and $u_\perp$ distributions, respectively. This is done as a function of the number of primary vertices n. The fitted Gaussian widths as a function of q_T for different number of primary vertices are parametrized by the following function,

$$\sigma(q_T; n) = \sqrt{N_n^2 + S_n^2 q_T}, \tag{5}$$

where N_n, S_n are parameters extracted from the fit. The average recoil and resolutions are extracted for both $Z/\gamma^* \to \mu^+\mu^-$ data and MC simulation, respectively.

The last step is to apply the average recoil and resolution extracted from $Z/\gamma^* \to \mu^+\mu^-$ events to improve the agreement of the $\not\!\!E_T$ distribution between data and MC simulation. As a self-closure test, in MC events the $\tilde{u}_{||}$ is shifted and parallel and perpendicular resolutions are scaled to match the average values of data. This is done on an event-by-event basis. The $\not\!\!E_T$ is then recalculated using the corrected $\vec{u}$ with Eq. 3. Figure 3 shows the $\not\!\!E_T$ and the Φ distributions of $\vec{\not\!\!E}_T$ ($\Phi(\not\!\!E_T)$) after applying the hadronic recoil correction. The data and MC simulation are in excellent agreement as expected. This demonstrates that this empirical correction to $\not\!\!E_T$ in the MC works very well for $Z/\gamma^* \to \mu^+\mu^-$ events. To apply the hadronic recoil correction determined

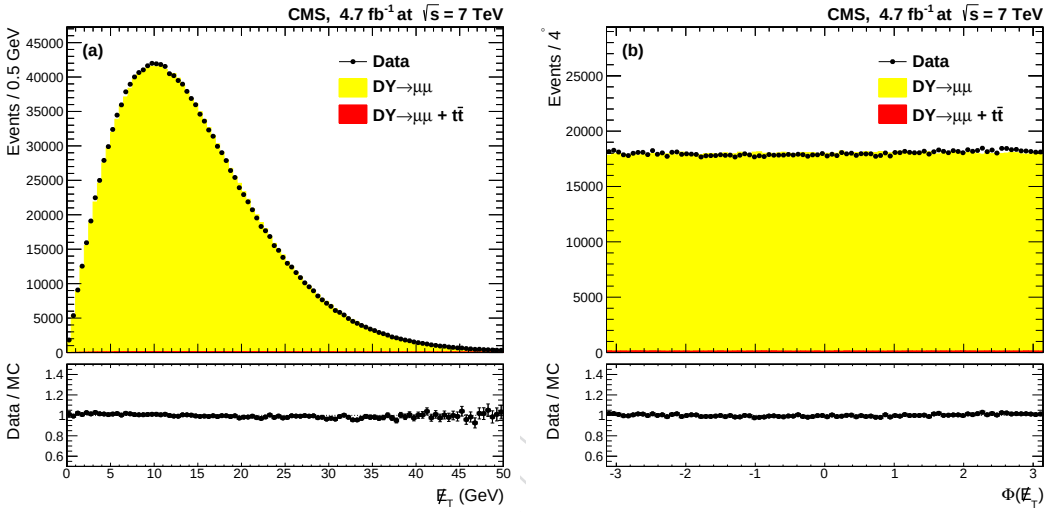

Figure 3: Data-MC comparison for $\not\!\!E_T$ (a) and Φ of the missing transverse momentum ($\Phi(\not\!\!E_T)$) (b) in the Drell-Yan control sample. Here, the hadronic recoil derived from the data was used to correct the MC simulation. The $Z/\gamma^* \to \tau^+\tau^- + t\bar{t}$ contribution in data is normalized to the data luminosity using a MC simulation, and the normalization of $Z/\gamma^* \to \mu^+\mu^-$ MC simulation is allowed to float so that the total number of simulated MC events is normalized to the data.

in $Z/\gamma^* \to \mu^+\mu^-$ events to other MC simulation, such as $W \to \mu\nu$ events, involves defining a variable equivalent to the boson $\vec{q_T}$ in $Z/\gamma^* \to \mu^+\mu^-$ events. With the properly defined $\vec{q_T}$, the hadronic recoil as defined in Eq. 2 is decomposed into $u_{||}$ and $u_\perp$ components relative to the $\vec{q_T}$, and the hadronic recoil correction is applied in the same way as in the $Z/\gamma^* \to \mu^+\mu^-$ MC simulation to correct for hadronic recoil and re-calculate the $\not\!\!E_T$. For the $W \to \mu\nu$ MC simulation, the vector sum of transverse momentum of reconstructed muon and the generated neutrino is defined to be the $\vec{q_T}$, while for $W \to \tau\nu$ events the generated W boson $\vec{q_T}$ is used. For Drell-Yan background events, which pass the Drell-Yan veto, the second muon could fail some of the muon quality selection criteria, or fall outside the detector acceptance. The vector sum of transverse momentum of the generator-level second muon and the reconstructed muon is defined to be the $\vec{q_T}$. For the QCD background, the $\vec{q_T}$ is defined to be the transverse momentum of the reconstructed muon. Figure 4 shows the $\not\!\!E_T$ distribution for the QCD control sample, where events were collected with a pre-scaled non-isolated muon trigger. Here we select events which fail the isolated muon trigger requirements. We also impose an anti-isolation selection cut $Iso_{trk}/p_T > 0.1$. For this QCD background dominated control sample, data and MC are in very good agreement after the application of the recoil corrections.

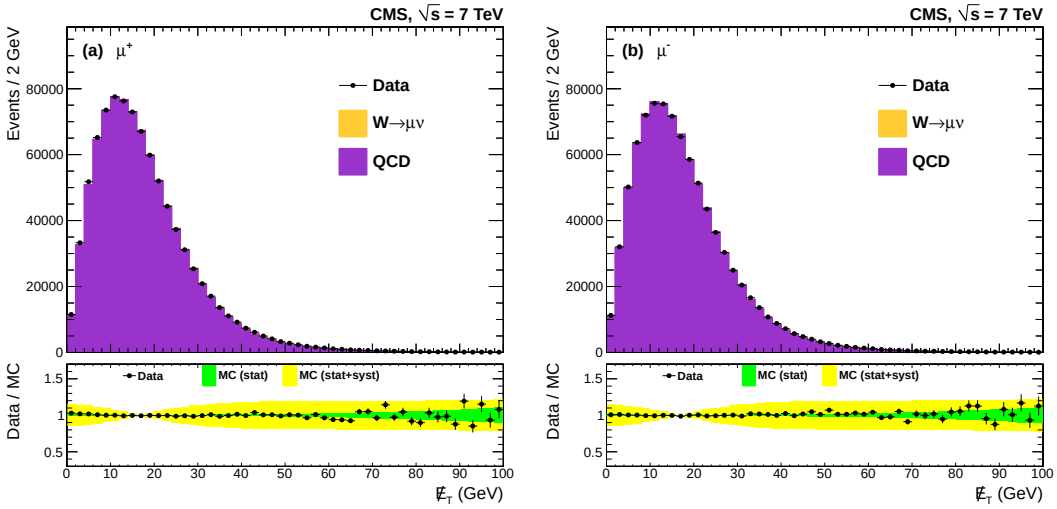

Figure 4: Data-MC comparison of the $\not\!\!E_T$ distribution for μ^+ ($\not\!\!E_T^+$) (a) , and μ^- ($\not\!\!E_T^-$) (b) in a QCD background dominated sample. The hadronic recoil derived from data was used to correct the MC simulation. The W $\rightarrow \mu\nu$ contribution in data is normalized to data luminosity using MC simulation and the normalization of the QCD simulation is allowed to float so that total number of MC simulated events is normalized to the data. The green band in each ratio plot shows the statistical uncertainty of the QCD MC $\not\!\!E_T$ shape and the yellow band shows the total uncertainty, including the systematic uncertainties due to QCD $\not\!\!E_T$ modeling as discussed in Section 6.

5.3 Extraction of the asymmetry from fits to the $\not\!\!E_T$ distributions

The W $\rightarrow \mu\nu$ signal is extracted from fits to the $\not\!\!E_T$ distributions of W $\rightarrow \mu\nu$ candidates as shown in Figure 5. Fits are shown for three $|\eta|$ bins: $0.0 \leq |\eta| < 0.2$, $1.0 \leq |\eta| < 1.2$, and $2.1 \leq |\eta| < 2.4$, respectively. The $\not\!\!E_T$ distributions for the W $\rightarrow \mu\nu$ signal and backgrounds are obtained from simulations which are corrected for the hadronic recoil as measured in $Z/\gamma^* \rightarrow \mu^+\mu^-$ events. The ratios between the data points and the final fits are shown on the bottom of each panel. Table 1 summarizes the fitted N^{W^+}, N^{W^-}, correlation between the uncertainties of the N^{W^+} and N^{W^-} ($\rho_{(N^{W^+},N^{W^-})}$), the $\mathcal{A}^{raw}$, and the χ^2 value of the fit for each $|\eta|$ bin. The χ^2 values show that the fit model describes the data well. Here, $\mathcal{A}^{raw}$ is calculated using Eq. 1. The correlation between the uncertainties in N^{W^+} and N^{W^-} are taken into account in the estimated error of $\mathcal{A}^{raw}$. This correlation is about 10–15% and varies from bin to bin. The extracted $\mathcal{A}^{raw}$ is further corrected for possible detector bias as discussed in the sections below.

We also repeat the analysis with a higher muon p_T threshold of 35 GeV. For this higher threshold, the lepton charge asymmetry is forced to be closer to the W-boson charge asymmetry due to kinematic constraints. Therefore, theoretical predictions for the asymmetry are different. For a higher muon p_T threshold, the background compositions are significantly different. The expected QCD background is reduced to about 1% in the W $\rightarrow \mu\nu$ candidate sample. The $p_T > 35$ GeV sample provides a cross check of the analysis method. Note that the W $\rightarrow \mu\nu$ candidates with $p_T > 35$ GeV are included in the measurement for $p_T > 25$ GeV. The results with muon p_T threshold of 35 GeV are also summarized in Table 1.

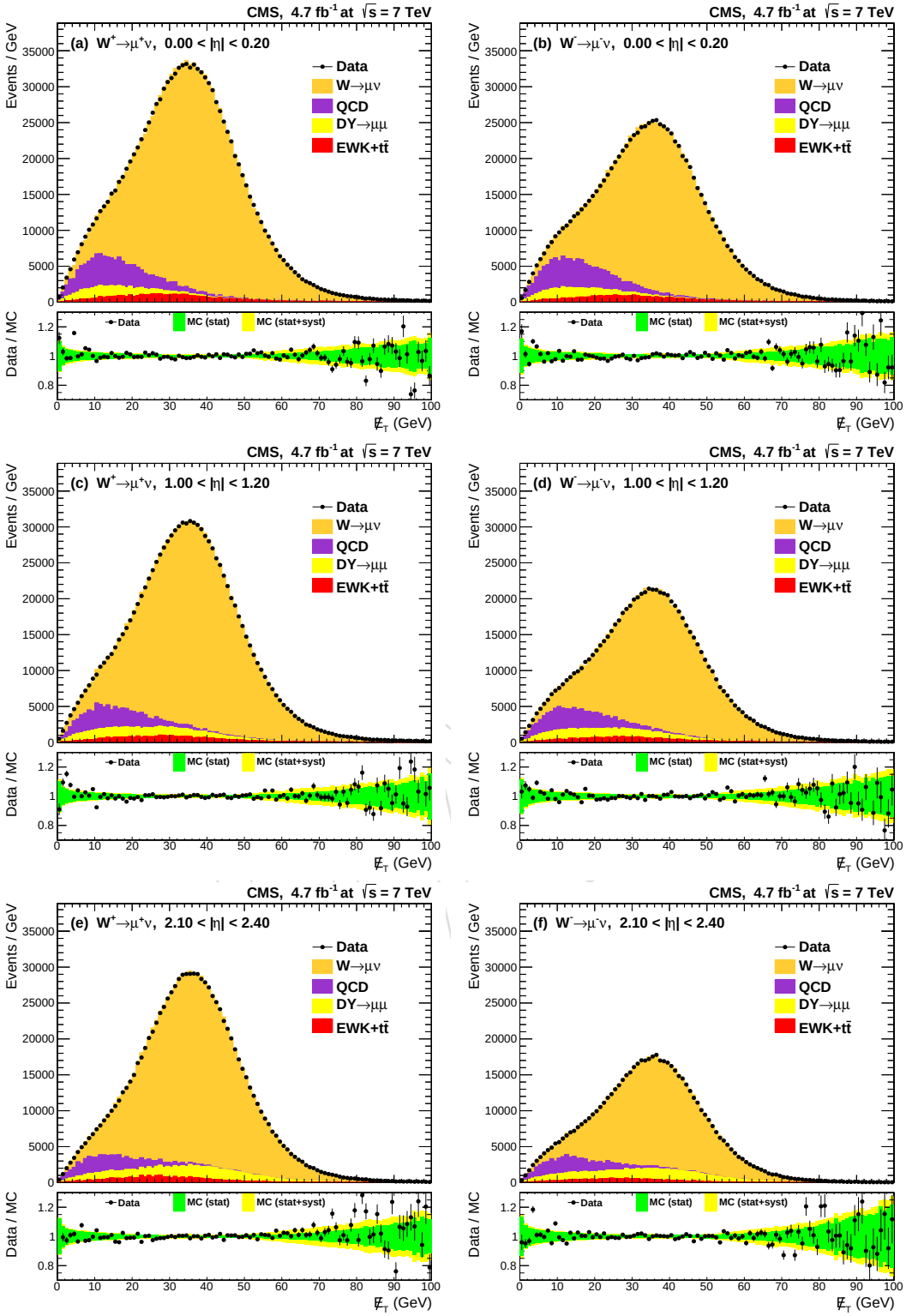

Figure 5: Muon $p_T > 25$ GeV data sample. Examples of the extraction of the W $\to \mu\nu$ signal from fits to $\not{E}_T$ distributions of W $\to \mu\nu$ candidates in data: $0.0 \leq |\eta| < 0.2$ (a, b), $1.0 \leq |\eta| < 1.2$ (c, d), and $2.1 \leq |\eta| < 2.4$ (e, f). The fits to $W^+ \to \mu^+\nu$ and $W^- \to \mu^-\bar{\nu}$ candidates are in sub-figure (a, c, e) and (b, d, f), respectively. The ratios between the data points and the final fits are shown on the bottom of each panel. The green band in each ratio plot shows the statistical uncertainty in the shape of the MC $\not{E}_T$ distribution, and the yellow band shows the total uncertainty, including all systematic uncertainties as discussed in Section 6.

Table 1: Summary of the fitted N^{W^+}, N^{W^-}, correlation between the uncertainties in N^{W^+} and N^{W^-} ($\rho_{(N^{W^+},N^{W^-})}$), χ^2 of the fit and the extracted $\mathcal{A}^{raw}$ for each $|\eta|$ bin. Here, $\rho_{(N^{W^+},N^{W^-})}$ and $\mathcal{A}^{raw}$ are in units of percent.

$\|\eta\|$ bin	N^{W^+} ($\times 10^3$)	N^{W^-} ($\times 10^3$)	$\rho_{(N^{W^+},N^{W^-})}$	χ^2 (NDF=197)	$\mathcal{A}^{raw}$ (%)
$p_T > 25$ GeV					
0.00-0.20	1033.0 ± 1.4	764.9 ± 1.2	14.5	255	14.912±0.096
0.20-0.40	970.2 ± 1.3	713.9 ± 1.2	14.9	190	15.216±0.098
0.40-0.60	1060.3 ± 1.4	771.5 ± 1.2	14.7	220	15.766±0.094
0.60-0.80	1055.1 ± 1.4	752.4 ± 1.2	14.6	213	16.745±0.093
0.80-1.00	935.8 ± 1.3	652.1 ± 1.1	14.5	245	17.866±0.098
1.00-1.20	931.0 ± 1.3	625.4 ± 1.1	13.9	231	19.636±0.099
1.20-1.40	949.0 ± 1.3	621.6 ± 1.1	14.2	209	20.848±0.099
1.40-1.60	957.1 ± 1.3	607.3 ± 1.1	13.7	202	22.365±0.099
1.60-1.85	1131.8 ± 1.4	687.6 ± 1.2	14.7	225	24.417±0.093
1.85-2.10	1113.4 ± 1.4	656.8 ± 1.1	12.9	237	25.797±0.094
2.10-2.40	843.6 ± 1.2	481.3 ± 1.0	11.8	244	27.341±0.106
$p_T > 35$ GeV					
0.00-0.20	574.3 ± 1.0	459.7 ± 0.9	18.9	203	11.083±0.116
0.20-0.40	538.9 ± 0.9	428.9 ± 0.9	17.4	202	11.371±0.119
0.40-0.60	588.3 ± 1.0	462.8 ± 0.9	18.5	187	11.935±0.114
0.60-0.80	582.9 ± 1.0	453.7 ± 0.9	18.7	205	12.472±0.114
0.80-1.00	513.7 ± 0.9	392.3 ± 0.8	18.7	218	13.406±0.124
1.00-1.20	509.1 ± 0.9	379.2 ± 0.8	15.7	226	14.620±0.121
1.20-1.40	520.2 ± 0.9	376.9 ± 0.8	16.2	191	15.970±0.123
1.40-1.60	522.7 ± 0.9	370.2 ± 0.8	14.7	195	17.074±0.123
1.60-1.85	614.6 ± 1.0	418.8 ± 0.9	17.5	239	18.945±0.118
1.85-2.10	604.7 ± 1.0	395.8 ± 0.9	15.0	192	20.885±0.123
2.10-2.40	464.3 ± 0.9	288.5 ± 0.8	14.7	234	23.357±0.141

6 Systematic uncertainties

In order to compare the experimental results to theoretical predictions, we investigate possible additional corrections to $\mathcal{A}^{raw}$ from detector bias that results in a difference from the true charge asymmetry ($\mathcal{A}^{true}$). For the MC simulation $\mathcal{A}^{true}$ is defined as the asymmetry at the generator level.

One possible bias can originate from muon charge mis-identification (w), which can dilute the charge asymmetry by a factor of $(1-2w)\cdot\mathcal{A}^{true}$. The muon charge misidentification rate has been studied in detail and shown to have negligible effect on the charge asymmetry [8]. The muon momentum resolution can also smear $\mathcal{A}^{true}$. The resolution on the measurement of muon momentum depends on η [23] and varies from 1.5 to 5.0%. The uncertainty on the muon momentum correction can also contribute an additional systematic uncertainty in the signal estimation as discussed below. The QED final-state-radiation (FSR) can reduce the muon p_T and result a difference in acceptance between W^+ and W^- for a given muon p_T selection. The effect of FSR on the muon charge asymmetry was previously studied using POWHEG MC

samples. It was found that FSR reduces the asymmetry by about 0.1% [8] for $W \to \mu\nu$ decays.

A difference in the efficiency for μ^+ and μ^- can bias the measured charge asymmetry. We can correct for a difference in the efficiency for μ^+ and μ^- events using the following expression,

$$\mathcal{A}^{true} = \mathcal{A}^{raw} - \frac{1-(\mathcal{A}^{raw})^2}{2}\left(r^{W^+/W^-} - 1\right), \tag{6}$$

where r^{W^+/W^-} is the ratio of the selection efficiency between W^+ and W^- events. The systematic uncertainty from a possible efficiency difference between the μ^+ and μ^- on the extraction of the $\mathcal{A}^{raw}$ is discussed below.

For studies of some of the systematic uncertainties, we generate a large number of pseudo-experiments and repeat the entire analysis for each pseudo-experiment. This method is used to determine the uncertainties in the asymmetry from the muon scale correction, event selection and from the $\not\!\!E_T$ correction. The resulting extracted raw charge asymmetries are used to determine corrections to the asymmetry and assign systematic uncertainties.

6.1 Efficiency ratio

As discussed previously, the muon offline and trigger efficiencies are measured in 7 bins in p_T and 22 bins in η bins for μ^+ and μ^-, respectively. The offline efficiency ratio between μ^+ and μ^- is very close to 1 in most of the detector regions. However, there is evidence that the ratio deviates from 1 in the transition regions between detectors.

We correct for the efficiency bias in the detector using the muon efficiencies extracted from the $Z/\gamma^* \to \mu^+\mu^-$ data and MC samples. For each $|\eta|$ bin an average W selection efficiency $\epsilon(W^\pm)$ is obtained from the following expression,

$$\epsilon(W^\pm) = \frac{\Sigma(k \cdot \epsilon^{\mu^\pm,\, data}(p_T,\eta)/\epsilon^{\mu^\pm,\, MC}(p_T,\eta))}{\Sigma(k/\epsilon^{\mu^\pm,\, MC}(p_T,\eta))}, \tag{7}$$

where $\epsilon^{\mu^\pm,\, data}(p_T,\eta)$, $\epsilon^{\mu^\pm,\, MC}(p_T,\eta)$ are total muon efficiencies and k are additional event-by-event weights introduced by W boson q_T reweighting described below. The PU difference between data and MC has been corrected for using the "accept-reject" technique based on data/MC PU distributions. The ratio (r^{W^+/W^-}) between $\epsilon(W^+)$ and $\epsilon(W^-)$ is used to correct for the raw charge asymmetry following Eq. 6. All MC samples are corrected for any data/MC efficiency difference.

To estimate the systematic uncertainty from the muon efficiencies, the muon efficiency values in data and MC simulation are modified according to their errors independently in each p_T–η bin. Many pseudo-efficiency tables are generated. In each pseudo-experiment the efficiency values are used to correct the MC simulation and measure the $\mathcal{A}^{raw}$. The $\mathcal{A}^{raw}$ is further corrected for W selection efficiency ratio r^{W^+/W^-} as described above. The RMS of the resulting asymmetry distribution is treated as the systematic error originating from the uncertainty in the determination of the ratio of the muon efficiencies. In this study, the variations for different $|\eta|$ bins are completely independent from each other. Therefore, the systematic uncertainty from uncertainties in the efficiency ratio are assumed to have zero correlation between different $|\eta|$ bins. This is one of the dominant systematic uncertainties.

As a cross check, Figure 6 shows a comparison of the measured muon charge asymmetry between positive pseudorapidity ($\eta > 0$) and negative pseudorapidity ($\eta < 0$) regions. This is done by performing identical measurement in 22 muon η bins. We find that the charge asymmetries for $\eta > 0$ and $\eta < 0$ are in very good agreement with each other.

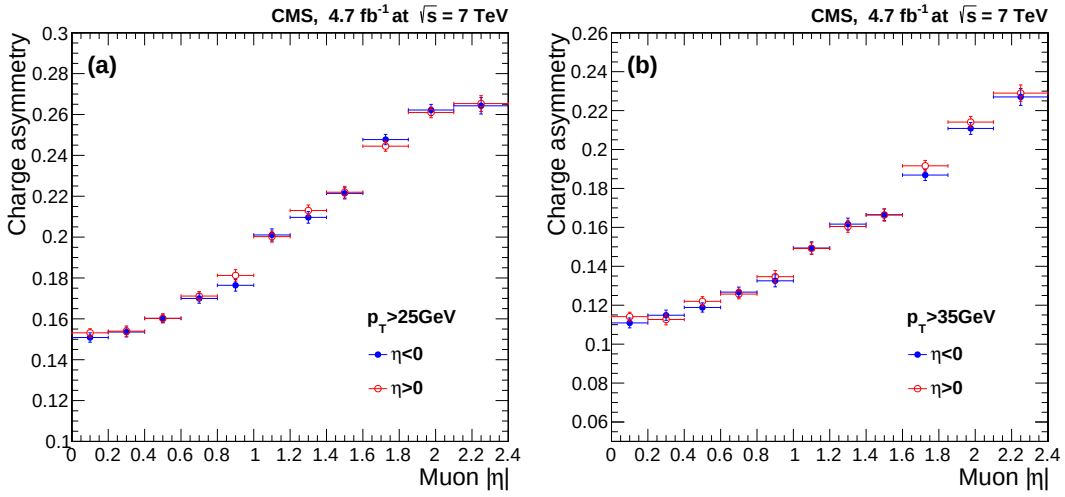

Figure 6: Comparison of the final muon charge asymmetry ($\mathcal{A}$) extracted for the positive pseudorapidity ($\eta > 0$) and negative pseudorapidity ($\eta < 0$) regions for the muon $p_{\mathrm{T}} > 25$ GeV (a) and muon $p_{\mathrm{T}} > 35$ GeV (b) samples. The uncertainties include only the statistical uncertainty from the signal extraction and uncertainty in the determination of the efficiencies for positive and negative muons.

6.2 Extraction of the signal of the W lepton charge asymmetry

The remaining systematic uncertainties in the extraction of the W lepton charge asymmetry originate from QCD background, correction for muon scale, QED FSR correction, PDF uncertainty, Drell-Yan background normalization, $\not\!\!E_{\mathrm{T}}$ modeling, PU reweighting, integrated luminosity, $\mathrm{t\bar{t}}$ and $\mathrm{W} \to \tau\nu$ background, and W boson q_T modeling. Among these systematic sources, the QCD background and correction for muon scale are the largest. In the following subsections each source of systematic uncertainty is discussed in detail and correlations between different $|\eta|$-bins are investigated to construct the correlation matrix among the total systematic uncertainties.

6.2.1 QCD background

The total QCD background normalization is allowed to float in the fit for the signal. The ratio of the QCD backgrounds in W^+ and W^- is fixed to the ratio observed in the QCD control region. There are two sources of the systematic error in the QCD background. The first is related to fixing the ratio of the backgrounds in the W^+ and W^- samples ("QCD +/-"), and the second is related to the modeling of the shape of the QCD $\not\!\!E_{\mathrm{T}}$ distribution ("QCD shape").

To evaluate the systematic uncertainty from "QCD +/-", the ratio is varied by $\pm 5\%$ and $\pm 15\%$ for muon p_{T} thresholds of 25 GeV and 35 GeV, respectively. The resulting shifts in the raw charge asymmetry are taken as one source of systematic error. For the last $|\eta|$ bin, this variation is 10% and 20%, respectively. These variations of the ratio span the maximum range indicated by the QCD MC simulation. As an additional cross check we fix the QCD shape to be the same for μ^+ and μ^- and allow the two QCD normalizations to float in the extraction of the signal. We find that the fitted values for the ratio of the QCD backgrounds for W^+ and W^- are within the variations quoted above. The bin–to–bin correlation of these uncertainties in the asymmetries is assumed to be zero.

The second source of systematic error is a possible difference in the shape of the QCD back-

ground for W^+ and W^-. The QCD $\not\!\!E_T$ shape is taken from the MC simulation and additional recoil correction is applied. Two types of variations in the shape of the QCD $\not\!\!E_T$ distribution are considered. First, the shape of the QCD $\not\!\!E_T$ distribution without the hadronic recoil correction is used in the extraction of the signal. This is done in a correlated way for the W^+ and W^- samples. Secondly, the shapes of the QCD $\not\!\!E_T$ distribution are varied separately for the W^+ and W^- samples (within the statistical uncertainty) and the resulting shapes are used in the signal extraction. The two contributions to the systematic uncertainties from the "QCD shape" are added in quadrature. The bin–to–bin correlation of the systematic uncertainties due to each shape variation is assumed to be 100%.

In total, the systematic uncertainty from the QCD backgrounds is comparable to the uncertainty from the determination of the muon efficiencies.

6.2.2 Muon momentum correction

The muon momentum correction affects both the yields and shapes of the $\not\!\!E_T$ distributions. To estimate the systematic error from this source the muon $1/p_T$ correction parameters in each $\eta - \phi$ bin and the muon scale global correction parameters are smeared within their errors 400 times. Each time the event yields can be slightly different in both data and MC, and the extraction of the asymmetry is done for each of the 400 cases. The RMS of the measured $\mathcal{A}^{raw}$ distribution in each muon $|\eta|$ bin is taken as systematic uncertainty and bin -to-bin correlations are zero.

The systematic uncertainty from the muon momentum correction is typically less than 40% of the error from the muon efficiency for the $p_T > 25$ GeV sample. However, the two errors are comparable for the $p_T > 35$ GeV sample for two reasons. First, the charge dependent bias from the alignment increases with p_T. Secondly the Jacobian peak of the $W \to \mu\nu$ events is close to 35 GeV.

6.2.3 QED FSR correction

We studied the impact of QED FSR to the muon charge asymmetry using the POWHEG $W \to \mu\nu$ MC sample. In this MC sample, FSR is implemented using a similar approach to parton showering and is approximate in LO. We compare the muon charge asymmetry prior and posterior FSR and the difference is found to be within 0.07-0.12% and 0.03-0.11% for muon p_T cuts of 25 GeV and 35 GeV, respectively. Recently, there are attempts to combine FSR, NLO electro-weak corrections and next-to-next-to-leading order (NNLO) QCD corrections for inclusive W/Z production and this has been done for Drell-Yan production [31]. For this measurement, the central values are not corrected for FSR. However, the full shift in the muon charge asymmetry predicted by the POWHEG MC is taken as an additional systematic uncertainty and the bin–to–bin correlation is assumed to be 100%.

6.2.4 PDF uncertainty

The PDF4LHC recommendation [32] is followed in the evaluation of the systematic uncertainties originating from uncertainties in PDF. The MSTW2008 [2], CT10 [3], and NNPDF2.1 [33] NLO PDF sets are used. All simulated events are reweighted to a given PDF set and the overall normalization is allowed to float. In this way both the uncertainties on the total cross-sections as well as in the shape of the $\not\!\!E_T$ distribution are considered. To estimate the systematic uncertainty for the uncertainties in CT10 and MSTW2008 PDFs, asymmetric master equations are used [2, 3]. For CT10 the 90% C.L. uncertainty is rescaled to 68% C.L. by dividing by a factor of 1.64485. For NNPDF2.3 PDF set the RMS of the $\mathcal{A}^{raw}$ distributions is taken. The half-width of

the maximum deviation from combining all three PDF uncertainty bands is taken as the PDF uncertainty. The CT10 error set is used to estimate the bin–to–bin correlations.

The PDF uncertainty is estimated to be about 10% of the total experimental uncertainty. The remaining sources of systematic errors are smaller and many are negligible.

6.2.5 Drell-Yan background

The $Z/\gamma^* \rightarrow \mu^+\mu^-$ events in the Drell-Yan control region are used to check the Drell-Yan normalization. This is done in several bins of dimuon invariant mass regions: [15, 30, 40, 60, 120, 150, inf] GeV. The $Z/\gamma^* \rightarrow \mu^+\mu^-$ MC simulation in each bin is compared to the data yields after correcting the MC for data/MC difference in PU, Z boson q_T, $\not\!\!E_{\rm T}$ modeling, and efficiencies. After correcting for the detector bias and physics mis-modeling, the MC simulation describes the data well, as shown in Figure 2 for dimuon invariant mass between [60, 120] GeV. The data yield in this bin is about 3% higher than the predictions from the NNLO cross section as calculated by FEWZ 3.1 [31].

The ratios of data to MC of the $Z/\gamma^* \rightarrow \mu^+\mu^-$ event yields as a function of dimuon mass are used to rescale the MC prediction of the Drell-Yan background. We take the shift in the raw charge asymmetry with and without this rescaling as the systematic uncertainty. This and the PDF uncertainty on the $Z/\gamma^* \rightarrow \mu^+\mu^-$ yields are considered as systematic uncertainty due to "Drell-Yan background normalization". This uncertainty is almost negligible at central $|\eta|$ bins and increases in the forward $|\eta|$ bins. The Drell-Yan background is larger in the forward region because of the lower efficiency of the "Drell-Yan veto" due to lower to detector coverage. The systematic uncertainty in the Drell-Yan background is assumed to have 100% correlation from bin to bin.

6.2.6 $\vec{E}_{\rm T}$ modeling

To evaluate the systematic uncertainty due to the Φ-modulation of $\vec{\not\!\!E}_{\rm T}$, the correction for the Φ-modulation is removed and the shift in the raw charge asymmetry is taken as the systematic uncertainty.

The hadronic recoil correction changes the shape of the $\not\!\!E_{\rm T}$ distribution of all MC samples. To calculate the systematic error from this source, the average recoil and resolution parameters are smeared within their uncertainties, taking into account the correlations between them. This is done 400 times and the RMS of the resulting $\mathcal{A}^{raw}$ distribution is taken as systematic uncertainty and bin–to–bin correlations are calculated.

6.2.7 Pile-up

Pile-up can affect the $\not\!\!E_{\rm T}$ shapes. To estimate the effect of mis-modeling of PU in the simulation, the minimum bias cross-section is varied by $\pm$5% and the PU distributions expected in data are re-generated. The MC simulation is then reweighted to match to data and the resulting shift in $\mathcal{A}^{raw}$ is treated as systematic uncertainty from PU. PU affects the $\not\!\!E_{\rm T}$ shapes for all muon pseudorapidity bins in the same direction with a correlation of 100%.

6.2.8 Integrated luminosity

The $Z/\gamma^* \rightarrow \tau^+\tau^-$ and $t\bar{t}$ backgrounds are normalized to the data luminosity after correcting for the muon efficiency difference between data and MC simulation. The uncertainty on the integrated luminosity is about 2.2%. The normalization of all the MC backgrounds is varied by

$\pm$2.2%, and the resulting maximum shift in $\mathcal{A}^{raw}$ is taken as systematic uncertainty from uncertainties in the determination of the luminosity. The bin–to–bin correlations in the measured asymmetries are +100%.

6.2.9 $t\bar{t}$ and $W \to \tau\nu$ background

An additional 15% is assigned as the uncertainty in the theoretical prediction [26] of the $t\bar{t}$ cross section and the bin–to–bin correlation of the resulting systematic uncertainty in the asymmetry is assumed to be 100%.

The $W \to \tau\nu$ background is normalized to the $W \to \mu\nu$ yields in data with a ratio obtained from a MC simulation. This ratio is largely determined by the branching fraction of τ decaying to μ. A 2% uncertainty is assigned to the $W \to \tau\nu$ to $W \to \mu\nu$ ratio [34]. Here, the bin–to–bin correlations in the measured asymmetries are 100%.

6.2.10 W boson q_T modeling

To improve the agreement between data and simulation, the W boson q_T spectrum is reweighted using weight factors which are the ratios of the distribution of boson q_T for $Z/\gamma^* \to \mu^+\mu^-$ events in data and MC simulation. Here we make the assumption that the scale factors to correct the boson q_T distribution in MC simulation to match the data are the same for W and Z events. This assumption is tested using two different sets of MC simulations: one from the POWHEG event generator and the other from MADGRAPH [35]. Here, MADGRAPH is treated as the "data", and the ratio of Z boson q_T between the MADGRAPH simulation and the POWHEG simulation is compared to the same ratio in simulated W events. This double ratio is parametrized using an empirical function to smooth the statistical fluctuations, and additional weights are obtained using the fitted function. Here we reweight the POWHEG simulation to be close to MADGRAPH simulation and measure the asymmetry again. The deviation of $\mathcal{A}^{raw}$ is taken as the systematic uncertainty due to mis-modeling of W boson q_T. The default boson q_T reweighting which is applied is based on the POWHEG simulation.

6.3 Total systematic uncertainty

Table 2 summarizes the total systematic uncertainty in each $|\eta|$ bin. For comparison, the statistical uncertainty in each $|\eta|$ bin is also shown in the same table. The dominant systematic uncertainty is from uncertainties in the muon efficiencies, QCD background, and muon scale correction. The correlation matrix of systematic uncertainty between different $|\eta|$ bins is summarized in Table 3. The correlations between different $|\eta|$ bins are small. The maximum correlation between different $|\eta|$ bins is about 37% and 14% for muon p_T threshold of 25 GeV and 35 GeV, respectively. Much of the correlation is due to the systematic uncertainty from QED FSR and QCD background.

7 Results and discussion

The measured asymmetries ($\mathcal{A}$) after all corrections are shown in Figure 7 and summarized in Table 4. Both statistical and systematic uncertainties are included. The asymmetries are compared to several PDF models. The theoretical predictions are obtained using FEWZ 3.1 [31] MC interfaced with CT10 [3], NNPDF2.3 [36], HERAPDF1.5 [37], MSTW2008 [2], and MSTW-2008CPDEUT [14] NLO PDF models. The numerical values of the theoretical predictions are also shown in Table 4. We also cross check the theoretical predictions using DYNNLO [38, 39] MC tool and the agreement between FEWZ 3.1 and DYNNLO is within 1%. The predictions

Table 2: Total systematic uncertainty in each $|\eta|$ bin. The statistical uncertainty in each $|\eta|$ bin is also shown for comparison. A detailed description of each systematic uncertainty is given in the text. The units are in percent, the same as for the asymmetry.

$\|\eta\|$ bin	0.0-0.2	0.2-0.4	0.4-0.6	0.6-0.8	0.8-1.0	1.0-1.2	1.2-1.4	1.4-1.6	1.6-1.85	1.85-2.1	2.1-2.4
$p_T > 25$ GeV											
Stat. unc.	0.096	0.098	0.094	0.093	0.098	0.099	0.099	0.099	0.093	0.094	0.106
Efficiency	0.111	0.133	0.121	0.122	0.170	0.175	0.170	0.168	0.165	0.175	0.268
QCD +/-	0.120	0.113	0.110	0.105	0.102	0.103	0.097	0.104	0.108	0.094	0.183
QCD shape	0.070	0.065	0.065	0.067	0.068	0.069	0.078	0.082	0.092	0.083	0.087
Muon scale	0.045	0.050	0.050	0.049	0.051	0.054	0.054	0.058	0.054	0.054	0.055
FSR	0.074	0.077	0.104	0.109	0.089	0.113	0.107	0.091	0.118	0.087	0.077
PDF	0.028	0.026	0.023	0.025	0.018	0.020	0.027	0.031	0.042	0.050	0.069
Drell-Yan bkg.	0.002	0.001	0.002	0.003	0.000	0.007	0.001	0.013	0.019	0.038	0.046
$\not{E}_T$ Φ modul.	0.011	0.009	0.033	0.012	0.029	0.034	0.044	0.045	0.055	0.049	0.038
Recoil	0.003	0.003	0.003	0.003	0.003	0.003	0.003	0.003	0.003	0.004	0.003
Pileup	0.017	0.013	0.011	0.005	0.014	0.025	0.022	0.031	0.019	0.028	0.000
Luminosity	0.002	0.003	0.004	0.004	0.006	0.009	0.012	0.017	0.024	0.033	0.040
$t\bar{t}$ bkg.	0.012	0.013	0.012	0.012	0.011	0.011	0.010	0.009	0.008	0.007	0.005
$W \to \tau\nu$ bkg.	0.026	0.026	0.026	0.026	0.026	0.025	0.025	0.025	0.025	0.025	0.024
W q_T	0.003	0.004	0.004	0.005	0.008	0.011	0.008	0.009	0.006	0.003	0.000
Total syst. unc.	0.203	0.212	0.217	0.216	0.238	0.255	0.251	0.250	0.266	0.256	0.364
Total unc.	0.225	0.233	0.236	0.235	0.258	0.274	0.270	0.269	0.282	0.273	0.379
$p_T > 35$ GeV											
Stat. unc.	0.116	0.119	0.114	0.114	0.124	0.121	0.123	0.123	0.118	0.123	0.141
Efficiency	0.120	0.138	0.116	0.107	0.159	0.164	0.171	0.176	0.186	0.194	0.325
QCD +/-	0.151	0.138	0.135	0.128	0.133	0.118	0.116	0.122	0.137	0.120	0.168
QCD shape	0.030	0.025	0.017	0.023	0.024	0.022	0.018	0.017	0.031	0.031	0.037
Muon scale	0.122	0.135	0.134	0.141	0.146	0.154	0.162	0.170	0.161	0.172	0.189
FSR	0.028	0.050	0.057	0.078	0.022	0.041	0.076	0.055	0.090	0.109	0.105
PDF	0.008	0.008	0.007	0.011	0.012	0.010	0.017	0.022	0.031	0.040	0.058
Drell-Yan bkg.	0.010	0.009	0.009	0.003	0.006	0.010	0.008	0.009	0.009	0.020	0.040
$\not{E}_T$ Φ modul.	0.002	0.009	0.010	0.003	0.008	0.028	0.037	0.035	0.022	0.022	0.001
Recoil	0.005	0.006	0.005	0.004	0.005	0.004	0.005	0.004	0.004	0.006	0.008
Pileup	0.015	0.003	0.005	0.018	0.019	0.002	0.007	0.003	0.013	0.014	0.032
Luminosity	0.001	0.002	0.000	0.000	0.000	0.001	0.004	0.010	0.016	0.025	0.039
$t\bar{t}$ bkg.	0.011	0.013	0.012	0.011	0.011	0.010	0.010	0.009	0.007	0.006	0.005
$W \to \tau\nu$ bkg.	0.013	0.012	0.013	0.012	0.012	0.012	0.011	0.012	0.011	0.011	0.011
W q_T	0.004	0.002	0.004	0.004	0.007	0.005	0.006	0.009	0.009	0.001	0.014
Total syst. unc.	0.234	0.245	0.232	0.234	0.258	0.261	0.278	0.283	0.301	0.313	0.436
Total unc.	0.261	0.272	0.259	0.260	0.286	0.288	0.304	0.308	0.323	0.336	0.458

using the CT10 PDF and HERAPDF1.5 parametrization are in good agreement with the data. The predictions using the NNPDF2.3 PDFs (which include the previous CMS electron charge asymmetry result [10] and other LHC experimental measurements in the fits) are also in good agreement with the data. The predictions using MSTW2008 PDF parametrization are in poor agreement with the data. The more recent MSTW2008CPDEUT PDF set is a variant of the MSTW2008 PDF set with a more flexible input parametrization and deuteron corrections [14]. This modification has significantly improved the agreement with the CMS data without including the LHC data, as shown in Figure 7.

Since the per-bin experimental total uncertainty is significantly smaller than the uncertainty in the current PDF parametrization this measurement can be used to reduce the uncertainties in the next generation of sets of PDFs.

Figure 8 shows a comparison of the measured muon charge asymmetries to NNLO predictions. The NNLO HERAPDF1.5 is used. The calculations are performed using both FEWZ 3.1 and

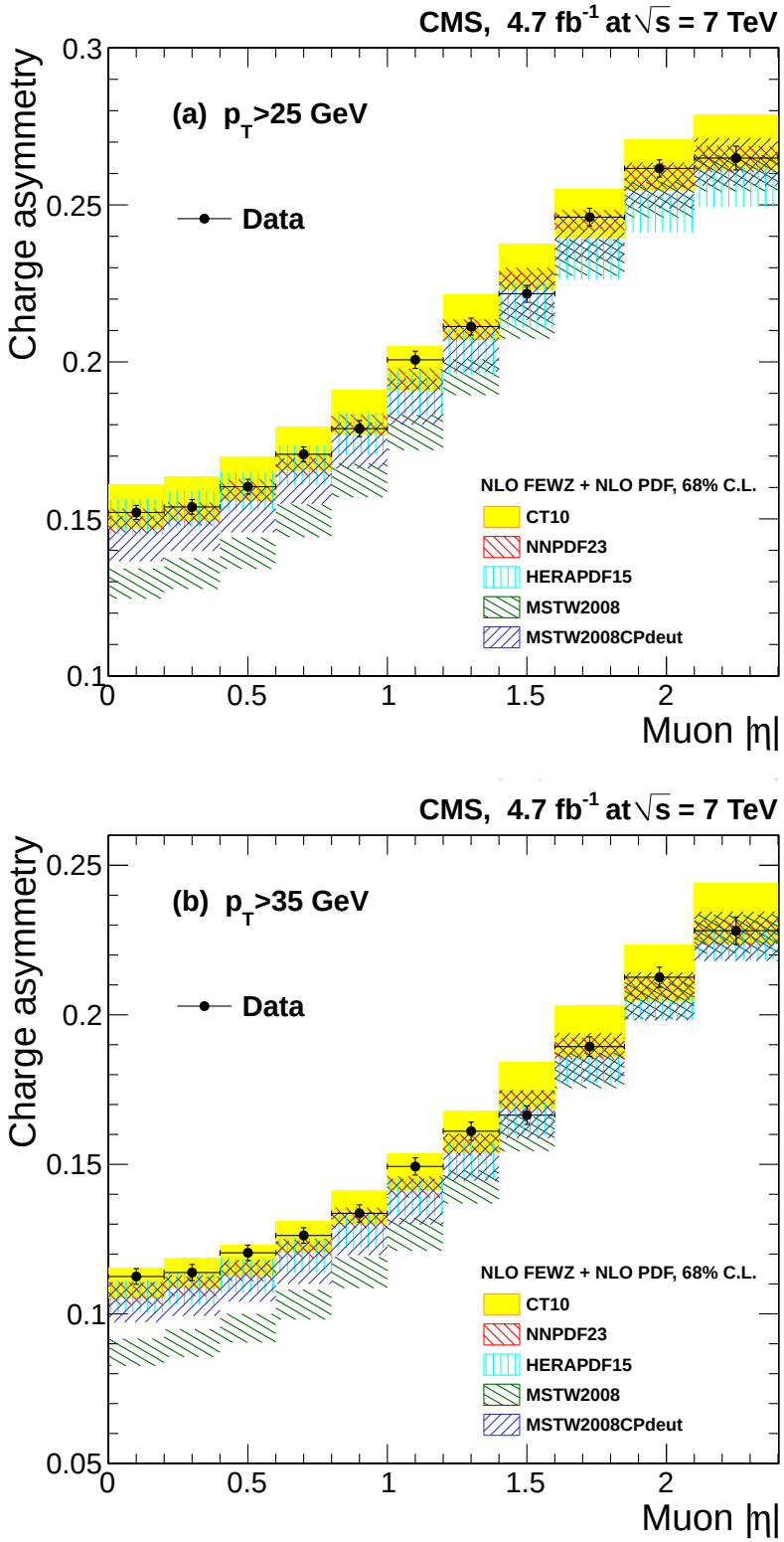

Figure 7: Comparison of the measured muon charge asymmetries to predictions with CT10 [3], NNPDF2.3 [36], HERAPDF1.5 [37], MSTW2008 [2], and MSTW2008CPDEUT [14] NLO PDF models. Results for muon $p_{\mathrm{T}} > 25$ GeV and muon $p_{\mathrm{T}} > 35$ GeV are shown in sub-figure (a) and (b), respectively. The error bars include both statistical and systematic uncertainties. The PDF uncertainty band corresponds to 68% confidence level (C.L.). The data points are shown at the center of each pseudorapidity bin. The theoretical predictions are calculated using the FEWZ 3.1 [31] MC.

Table 3: Correlation matrix of systematic uncertainties between different $|\eta|$ bins. The units are in percent.

$\|\eta\|$ bin	0.0-0.2	0.2-0.4	0.4-0.6	0.6-0.8	0.8-1.0	1.0-1.2	1.2-1.4	1.4-1.6	1.6-1.85	1.85-2.1	2.1-2.4
$p_T > 25$ GeV											
0.00-0.20	100.0	28.1	32.4	32.9	27.1	29.0	29.5	28.0	30.5	26.1	16.7
0.20-0.40		100.0	30.7	31.4	25.6	27.5	27.9	26.3	28.9	24.5	15.8
0.40-0.60			100.0	37.4	30.9	33.8	34.5	32.1	36.1	30.3	19.3
0.60-0.80				100.0	31.1	34.0	34.4	32.0	36.3	30.4	20.0
0.80-1.00					100.0	28.5	29.5	28.0	31.2	26.9	17.3
1.00-1.20						100.0	32.6	31.1	34.8	30.2	19.3
1.20-1.40							100.0	32.8	36.9	32.2	20.8
1.40-1.60								100.0	36.0	32.7	21.3
1.60-1.85									100.0	37.1	24.9
1.85-2.10										100.0	24.4
2.10-2.40											100.0
$p_T > 35$ GeV											
0.00-0.20	100.0	4.6	4.8	6.4	3.4	3.6	4.7	3.4	5.4	5.8	4.3
0.20-0.40		100.0	6.4	8.5	3.3	4.3	6.3	4.4	7.2	8.0	5.8
0.40-0.60			100.0	9.8	3.8	5.6	8.4	6.2	8.9	9.9	6.6
0.60-0.80				100.0	5.1	6.9	10.7	7.8	11.9	13.5	9.7
0.80-1.00					100.0	3.2	4.2	3.3	4.7	5.0	3.6
1.00-1.20						100.0	7.0	5.4	7.0	7.5	4.7
1.20-1.40							100.0	8.1	10.8	12.0	7.8
1.40-1.60								100.0	8.8	9.9	6.7
1.60-1.85									100.0	14.2	10.3
1.85-2.10										100.0	12.6
2.10-2.40											100.0

DYNNLO MC. Both MC give consistent result with agreement up to 1% level. At 25 GeV threshold, the predictions between NLO and NNLO are very similar. The NNLO predictions are slightly higher in high η regions. In the same η region, at 35 GeV threshold the NNLO predictions are significantly lower than the prediction at NLO. However, they agree well within the quoted PDF uncertainty in the HERAPDF1.5 PDFs.

Figure 9 shows a comparison of this result to previous CMS lepton charge asymmetry measurements. For most of the data points, the agreement is within one standard derivation. Note that in the previous lepton charge asymmetry results [8] [11], the central values were not corrected for any difference in efficiency between positive and negative muons (which is done for this result), but the statistical uncertainty in the determination of the efficiency ratio was included in the total systematic error. The data sample used in the previous CMS muon charge asymmetry measurement [11] is included in the dataset used here. Therefore, this result supersedes this previous measurement. The electron charge asymmetry extracted from part of the 2011 CMS data [10] uses a statistically independent data sample from this result. A combination of both results can be used to improve the constraints in PDF global fits. The correlation between the electron charge asymmetry and this result is expected to be small. The completely correlated systematic sources of error include the luminosity measurement, $t\bar{t}$ background, $W \to \tau\nu$ background, and PDF uncertainty.

The theoretical predictions for the lepton charge asymmetry are given for the kinematic region specified by the lepton p_T threshold. The acceptance is affected by the modeling of the W boson p_T which affects the prediction for the charge asymmetry. However, the effect on W^+ and W^- is largely correlated in the same direction. Therefore, the impact on the lepton charge asymmetry measurement cancels to first order. Figure 10 shows the comparison of these results to

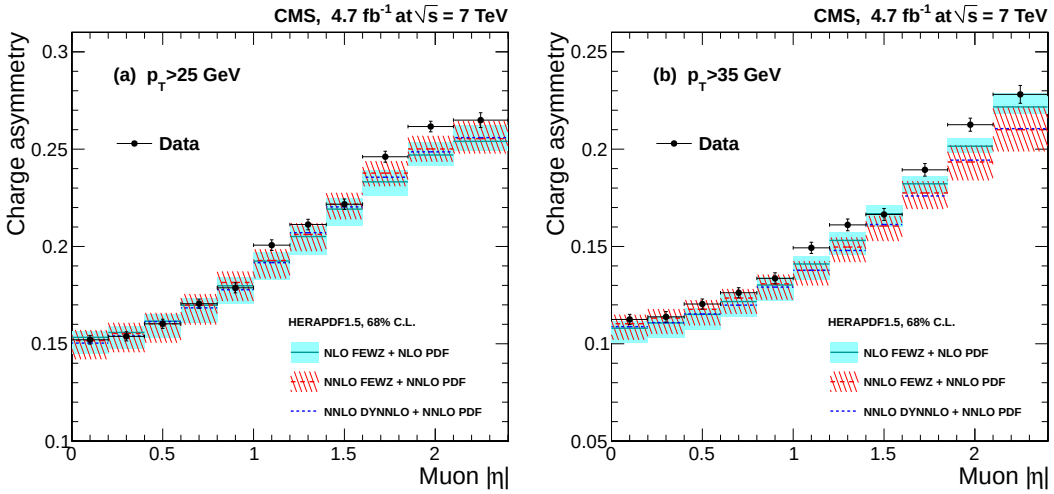

Figure 8: Comparison of the measured muon charge asymmetries to NNLO predictions for muon $p_{\mathrm{T}} > 25$ GeV (a) and muon $p_{\mathrm{T}} > 35$ GeV (b). The NNLO HERAPDF1.5 [37] has been used in NNLO calculations. The calculations are performed using both FEWZ 3.1 [31] and DYNNLO [38, 39] MC. The NLO prediction based on FEWZ 3.1 is also shown here.

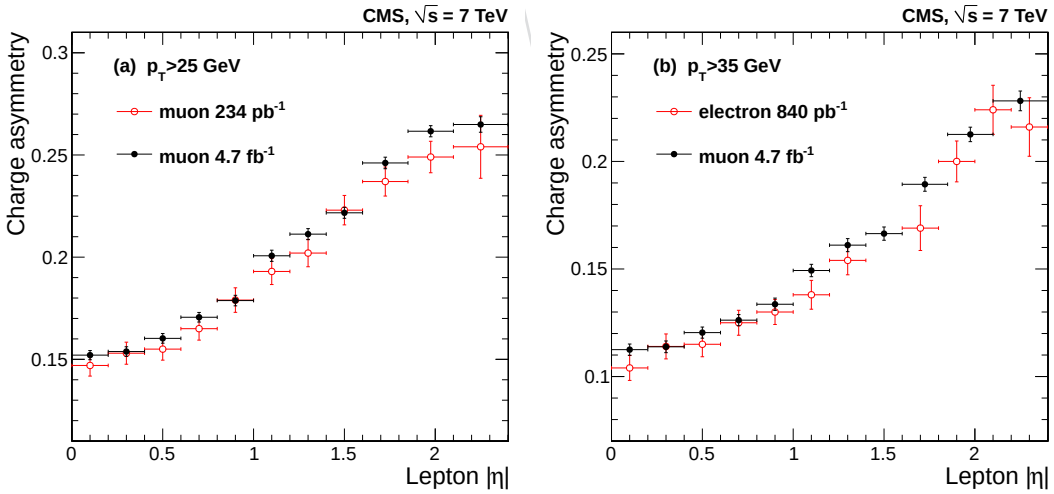

Figure 9: Comparison of this measurement to previous CMS lepton charge asymmetry results [10] [11]. Results are shown for muon $p_{\mathrm{T}} > 25$ GeV (a) and muon $p_{\mathrm{T}} > 35$ GeV (b).

Table 4: Summary of the final results for muon charge asymmetry ($\mathcal{A}$). The first uncertainty is statistical and the second is systematic. The theoretical predictions are obtained using FEWZ 3.1 [31] MC interfaced with CT10 [3], NNPDF2.3 [36], HERAPDF1.5 [37], and MSTW2008-CPDEUT [14] NLO PDF models. The PDF uncertainty is at 68% C.L. For each pseudorapidity bin the theoretical prediction is calculated using the averaged differential cross sections for positively and negatively charged leptons respectively. The units are in percent.

$\lvert\eta\rvert$	$\mathcal{A}$ ($\pm$stat.$\pm$syst.)	CT10	NNPDF2.3	HERAPDF1.5	MSTW2008CPDEUT
		$p_{\mathrm{T}} > 25$ GeV			
0.00-0.20	$15.21 \pm 0.10 \pm 0.20$	$15.35^{+0.74}_{-0.68}$	14.94 ± 0.39	$15.33^{+0.30}_{-0.84}$	$14.34^{+0.75}_{-0.69}$
0.20-0.40	$15.38 \pm 0.10 \pm 0.21$	$15.63^{+0.73}_{-0.69}$	15.16 ± 0.37	$15.58^{+0.32}_{-0.85}$	$14.67^{+0.75}_{-0.69}$
0.40-0.60	$16.03 \pm 0.09 \pm 0.22$	$16.27^{+0.71}_{-0.70}$	15.90 ± 0.36	$16.16^{+0.34}_{-0.88}$	$15.27^{+0.75}_{-0.70}$
0.60-0.80	$17.06 \pm 0.09 \pm 0.22$	$17.27^{+0.68}_{-0.71}$	16.71 ± 0.34	$16.98^{+0.37}_{-0.91}$	$16.19^{+0.74}_{-0.71}$
0.80-1.00	$17.88 \pm 0.10 \pm 0.24$	$18.45^{+0.66}_{-0.74}$	17.99 ± 0.33	$17.98^{+0.42}_{-0.94}$	$17.33^{+0.74}_{-0.73}$
1.00-1.20	$20.07 \pm 0.10 \pm 0.26$	$19.85^{+0.64}_{-0.76}$	19.46 ± 0.33	$19.25^{+0.48}_{-0.95}$	$18.74^{+0.73}_{-0.74}$
1.20-1.40	$21.13 \pm 0.10 \pm 0.25$	$21.50^{+0.63}_{-0.80}$	21.03 ± 0.33	$20.51^{+0.54}_{-0.92}$	$20.45^{+0.72}_{-0.76}$
1.40-1.60	$22.17 \pm 0.10 \pm 0.25$	$23.13^{+0.64}_{-0.84}$	22.66 ± 0.34	$21.92^{+0.59}_{-0.84}$	$22.12^{+0.70}_{-0.78}$
1.60-1.85	$24.61 \pm 0.09 \pm 0.27$	$24.87^{+0.65}_{-0.89}$	24.49 ± 0.35	$23.32^{+0.63}_{-0.70}$	$24.01^{+0.68}_{-0.79}$
1.85-2.10	$26.16 \pm 0.09 \pm 0.26$	$26.42^{+0.67}_{-0.95}$	25.88 ± 0.38	$24.70^{+0.65}_{-0.57}$	$25.70^{+0.65}_{-0.81}$
2.10-2.40	$26.49 \pm 0.11 \pm 0.36$	$27.13^{+0.74}_{-1.03}$	26.46 ± 0.42	$25.40^{+0.81}_{-0.48}$	$26.48^{+0.65}_{-0.87}$
		$p_{\mathrm{T}} > 35$ GeV			
0.00-0.20	$11.25 \pm 0.12 \pm 0.23$	$11.00^{+0.52}_{-0.48}$	10.68 ± 0.37	$10.80^{+0.32}_{-0.76}$	$10.39^{+0.67}_{-0.67}$
0.20-0.40	$11.38 \pm 0.12 \pm 0.24$	$11.36^{+0.52}_{-0.49}$	10.91 ± 0.33	$11.07^{+0.33}_{-0.77}$	$10.61^{+0.68}_{-0.68}$
0.40-0.60	$12.04 \pm 0.11 \pm 0.23$	$11.80^{+0.52}_{-0.50}$	11.40 ± 0.31	$11.51^{+0.34}_{-0.79}$	$11.10^{+0.70}_{-0.69}$
0.60-0.80	$12.62 \pm 0.11 \pm 0.23$	$12.59^{+0.53}_{-0.53}$	12.18 ± 0.33	$12.17^{+0.36}_{-0.80}$	$11.71^{+0.72}_{-0.71}$
0.80-1.00	$13.36 \pm 0.12 \pm 0.26$	$13.60^{+0.55}_{-0.58}$	13.21 ± 0.35	$13.02^{+0.37}_{-0.82}$	$12.70^{+0.74}_{-0.74}$
1.00-1.20	$14.93 \pm 0.12 \pm 0.26$	$14.79^{+0.59}_{-0.64}$	14.24 ± 0.36	$14.10^{+0.40}_{-0.81}$	$13.75^{+0.77}_{-0.77}$
1.20-1.40	$16.11 \pm 0.12 \pm 0.28$	$16.14^{+0.64}_{-0.73}$	15.65 ± 0.36	$15.31^{+0.41}_{-0.77}$	$15.24^{+0.79}_{-0.79}$
1.40-1.60	$16.64 \pm 0.12 \pm 0.28$	$17.72^{+0.70}_{-0.83}$	17.11 ± 0.36	$16.68^{+0.40}_{-0.68}$	$16.69^{+0.79}_{-0.82}$
1.60-1.85	$18.94 \pm 0.12 \pm 0.30$	$19.53^{+0.77}_{-0.94}$	18.87 ± 0.36	$18.22^{+0.40}_{-0.51}$	$18.62^{+0.77}_{-0.86}$
1.85-2.10	$21.26 \pm 0.12 \pm 0.31$	$21.52^{+0.82}_{-1.06}$	20.89 ± 0.38	$20.15^{+0.41}_{-0.32}$	$20.71^{+0.71}_{-0.90}$
2.10-2.40	$22.81 \pm 0.14 \pm 0.44$	$23.53^{+0.86}_{-1.17}$	22.73 ± 0.42	$22.17^{+0.71}_{-0.33}$	$22.79^{+0.66}_{-0.99}$

CT10NLO predictions based on FEWZ 3.1 and RESBOS [40–42]. RESBOS does a resummation in boson q_T at approximate next-to-next-to-leading logarithm which yields a more realistic description of boson q_T than a fixed-order calculation such as FEWZ 3.1. However, the difference between FEWZ 3.1 and RESBOS is negligible, and our measurement is not sensitive to the small difference between a fixed-order calculation and a boson q_T resummed prediction.

8 Summary

In summary, the W $\to \mu\nu$ lepton charge asymmetry is measured using a data sample corresponding to an integrated luminosity of 4.7 fb^{-1} collected with the CMS detector at the LHC (a sample of more than 20M W $\to \mu\nu$ events). The asymmetry is measured in 11 bins in absolute muon pseudorapidity for two different muon p_{T} thresholds: 25 GeV and 35 GeV. Compared to the previous CMS measurement, this measurement significantly reduces both the statistical and systematic uncertainties. The total uncertainty per bin is 0.2-0.4%. The data are in good agreement with the CT10, NNPDF2.3, and HERAPDF1.5 PDF parametrization. The data

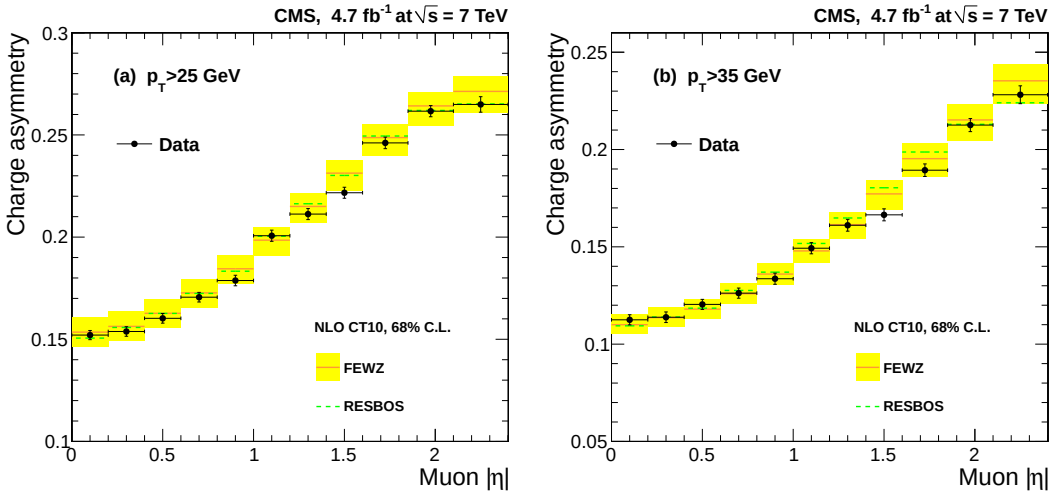

Figure 10: Comparison of the measured muon charge asymmetry to theoretical predictions based on FEWZ 3.1 and RESBOS MC calculations. The CT10 NLO PDF is used in both predictions. Results are shown for muon $p_{\mathrm{T}} > 25$ GeV (a) and muon $p_{\mathrm{T}} > 35$ GeV (b) .

are in poor agreement with the MSTW2008 parametrization, however the agreement has been significantly improved with the MSTW2008CPDEUT PDF set. The experimental errors are smaller than the current PDF uncertainties in the predictions. Therefore, this measurement can be used to significantly improve the determination of PDFs in future fits.

Acknowledgments

We wish to thank Graeme Watt for very useful discussions on MSTW PDF models, Frank Petriello for help with FEWZ MC tool, and C.P.-Yuan and Marco Guzzi for providing theoretical predictions based on RESBOS. We congratulate our colleagues in the CERN accelerator departments for the excellent performance of the LHC and thank the technical and administrative staffs at CERN and at other CMS institutes for their contributions to the success of the CMS effort. In addition, we gratefully acknowledge the computing centres and personnel of the Worldwide LHC Computing Grid for delivering so effectively the computing infrastructure essential to our analyses. Finally, we acknowledge the enduring support for the construction and operation of the LHC and the CMS detector provided by the following funding agencies: BMWF and FWF (Austria); FNRS and FWO (Belgium); CNPq, CAPES, FAPERJ, and FAPESP (Brazil); MEYS (Bulgaria); CERN; CAS, MoST, and NSFC (China); COLCIENCIAS (Colombia); MSES (Croatia); RPF (Cyprus); MoER, SF0690030s09 and ERDF (Estonia); Academy of Finland, MEC, and HIP (Finland); CEA and CNRS/IN2P3 (France); BMBF, DFG, and HGF (Germany); GSRT (Greece); OTKA and NKTH (Hungary); DAE and DST (India); IPM (Iran); SFI (Ireland); INFN (Italy); NRF and WCU (Republic of Korea); LAS (Lithuania); CINVESTAV, CONACYT, SEP, and UASLP-FAI (Mexico); MSI (New Zealand); PAEC (Pakistan); MSHE and NSC (Poland); FCT (Portugal); JINR (Armenia, Belarus, Georgia, Ukraine, Uzbekistan); MON, RosAtom, RAS and RFBR (Russia); MSTD (Serbia); SEIDI and CPAN (Spain); Swiss Funding Agencies (Switzerland); NSC (Taipei); ThEPCenter, IPST and NSTDA (Thailand); TUBITAK and TAEK (Turkey); NASU (Ukraine); STFC (United Kingdom); DOE and NSF (USA).

Individuals have received support from the Marie-Curie programme and the European Research Council (European Union); the Leventis Foundation; the A. P. Sloan Foundation; the

Alexander von Humboldt Foundation; the Belgian Federal Science Policy Office; the Fonds pour la Formation à la Recherche dans l'Industrie et dans l'Agriculture (FRIA-Belgium); the Agentschap voor Innovatie door Wetenschap en Technologie (IWT-Belgium); the Ministry of Education, Youth and Sports (MEYS) of Czech Republic; the Council of Science and Industrial Research, India; the Compagnia di San Paolo (Torino); and the HOMING PLUS programme of Foundation for Polish Science, cofinanced from European Union, Regional Development Fund.

References

[1] CMS Collaboration, "Measurements of Inclusive W and Z Cross Sections in pp Collisions at $\sqrt{s} = 7$ TeV", *JHEP* **1101** (2011) 080, doi:10.1007/JHEP01(2011)080, arXiv:1012.2466.

[2] A. D. Martin, W. J. Stirling, R. S. Thorne et al., "Parton distributions for the LHC", *Eur. Phys. J.* **C63** (2009) 189–285, doi:10.1140/epjc/s10052-009-1072-5, arXiv:0901.0002.

[3] H.-L. Lai et al., "New parton distributions for collider physics", *Phys. Rev.* **D82** (2010) 074024, doi:10.1103/PhysRevD.82.074024, arXiv:1007.2241.

[4] J. D. Björken and E. A. Paschos, "Inelastic electron proton and gamma proton scattering, and the structure of the nucleon", *Phys. Rev.* **185** (1969) 1975–1982, doi:10.1103/PhysRev.185.1975.

[5] CDF Collaboration, "Direct measurement of the W production charge asymmetry in $p\bar{p}$ Collisions at $\sqrt{s} = 1.96$ TeV", *Phys. Rev. Lett.* **102** (2009) 181801, doi:10.1103/PhysRevLett.102.181801, arXiv:0901.2169.

[6] D0 Collaboration, "Measurement of the electron charge asymmetry in $p\bar{p} \to W + X \to e\nu + X$ events at $\sqrt{s} = 1.96$ TeV", *Phys. Rev. Lett.* **101** (2008) 211801, doi:10.1103/PhysRevLett.101.211801, arXiv:0807.3367.

[7] ATLAS Collaboration, "Measurement of the Muon Charge Asymmetry from W Bosons Produced in pp Collisions at $\sqrt{s} = 7$ TeV with the ATLAS detector", *Phys.Lett. B* **701** (2011) 31, doi:10.1016/j.physletb.2011.05.024, arXiv:1103.2929v1.

[8] CMS Collaboration, "Measurement of the lepton charge asymmetry in inclusive W production in pp collisions at $\sqrt{s} = 7$ TeV", *JHEP* **04** (2011) 050, doi:10.1007/JHEP04(2011)050, arXiv:1103.3470v1.

[9] LHCb Collaboration, "Inclusive W and Z production in the forward region at $\sqrt{s} = 7$ TeV", *JHEP* **06** (2012) 058, doi:10.1007/JHEP06(2012)058, arXiv:1204.1620v3.

[10] CMS Collaboration, "Measurement of the electron charge asymmetry in inclusive W production in pp collisions at $\sqrt{s} = 7$ TeV", *Phys.Rev.Lett.* **109** (2012) 111806, doi:10.1103/PhysRevLett.109.111806, arXiv:1206.2598.

[11] CMS Collaboration, "Measurement of the muon charge asymmetry in inclusive W production in pp collisions at $\sqrt{s} = 7$ TeV", *CMS PAS* **EWK-11-005** (2011).

[12] R. D. Ball, V. Bertone, F. Cerutti et al., "Reweighting and Unweighting of Parton Distributions and the LHC W lepton asymmetry data", *Nucl.Phys.* **B855** (2012) 608–638, doi:10.1016/j.nuclphysb.2011.10.018, arXiv:1108.1758.

[13] S. Alekhin, J. Bluemlein, and S. Moch, "PDF fit in the fixed-flavor-number scheme", arXiv:hep-ph/1202.4642.

[14] A. Martin, A. T. Mathijssen, W. Stirling et al., "Extended Parameterisations for MSTW PDFs and their effect on Lepton Charge Asymmetry from W Decays", *Eur.Phys.J.* **C73** (2013) 2318, doi:10.1140/epjc/s10052-013-2318-9, arXiv:1211.1215.

[15] CMS Collaboration, "The CMS experiment at the CERN LHC", *JINST* **03** (2008) S08004, doi:10.1088/1748-0221/3/08/S08004.

[16] CMS Collaboration, "Particle-flow commissioning with muons and electrons from J/Ψ, and W events at 7 TeV", *CMS PAS* **PFT-2010-003** (2010).

[17] S. Frixione, P. Nason, and C. Oleari, "Matching NLO QCD computations with parton shower simulations: the POWHEG method", *JHEP* **11** (2007) 070, doi:10.1088/1126-6708/2007/11/070, arXiv:0709.2092.

[18] Z. Was, "TAUOLA the library for tau lepton decay, and KKMC / KORALB / KORALZ /... status report", *Nucl.Phys.Proc.Suppl.* **98** (2001) 96–102, doi:10.1016/S0920-5632(01)01200-2, arXiv:hep-ph/0011305.

[19] T. Sjöstrand, S. Mrenna, and P. Z. Skands, "PYTHIA 6.4 physics and manual", *JHEP* **05** (2006) 026, doi:10.1088/1126-6708/2006/05/026, arXiv:hep-ph/0603175.

[20] J. Pumplin et al., "New generation of parton distributions with uncertainties from global QCD analysis", *JHEP* **07** (2002) 012, doi:10.1088/1126-6708/2002/07/012, arXiv:hep-ph/0201195.

[21] GEANT4 Collaboration, "GEANT4: a simulation toolkit", *Nucl. Instrum. Meth.* **A506** (2003) 250–303, doi:10.1016/S0168-9002(03)01368-8.

[22] CMS Collaboration, "Performance of muon identification in pp collisions at $\sqrt{s}$=7 TeV", *CMS PAS* **MUO-10-002** (2010).

[23] CMS Collaboration, "Performance of muon identification in pp collisions at $\sqrt{s}$=7 TeV", *JINST* **7** (2012) P10002, doi:10.1088/1748-0221/7/10/P10002.

[24] A. Bodek, A. van Dyne, J.Y. Han, W. Sakumoto, and A. Strelnikov, "Extracting muon momentum scale corrections for hadron collider experiments", *Eur. Phys. J. C 72, 10* (2012).

[25] R. Barlow and C. Beeston, "Fitting using finite Monte Carlo samples", *Comp. Phys. Comm.* **77** (1993) 219–228.

[26] J. M. Campbell and R. K. Ellis, "Radiative corrections to Zb$\bar{\text{b}}$ production", *Phys. Rev.* **D62** (2000) 114012, doi:10.1103/PhysRevD.62.114012, arXiv:hep-ph/0006304.

[27] CDF Collaboration, "First run II measurement of the *W* boson mass at the Fermilab Tevatron", *Phys. Rev. D* **77** (2008) 112001, doi:10.1103/PhysRevD.77.112001.

[28] D0 Collaboration, "A Novel method for modeling the recoil in W boson events at hadron collider", *Nucl.Instrum.Meth.* **A609** (2009) 250–262, doi:10.1016/j.nima.2009.08.056, arXiv:0907.3713.

[29] CMS Collaboration, "CMS MET performance in events containing electroweak bosons from pp Collisions at $\sqrt{s}$=7 TeV", *CMS PAS* **JME-2010-005** (2010).

[30] M. Cacciari, G. P. Salam, and G. Soyez, "The anti-k_t jet clustering algorithm", *JHEP* **04** (2008) 063, doi:10.1088/1126-6708/2008/04/063, arXiv:0802.1189.

[31] Y. Li and F. Petriello, "Combining QCD and electroweak corrections to dilepton production in FEWZ", arXiv:1208.5967.

[32] M. Botje, J. Butterworth, A. Cooper-Sarkar et al., "The PDF4LHC Working Group Interim Recommendations", arXiv:1101.0538.

[33] R. D. Ball, V. Bertone, F. Cerutti et al., "Impact of Heavy Quark Masses on Parton Distributions and LHC Phenomenology", *Nucl.Phys.* **B849** (2011) 296–363, doi:10.1016/j.nuclphysb.2011.03.021, arXiv:1101.1300.

[34] Particle Data Group Collaboration, "Review of Particle Physics", *Phys. Rev. D* **86** (2012) 010001, doi:10.1103/PhysRevD.86.010001.

[35] J. Alwall, M. Herquet, F. Maltoni et al., "MadGraph 5 : Going Beyond", *JHEP* **1106** (2011) 128, doi:10.1007/JHEP06(2011)128, arXiv:1106.0522.

[36] R. D. Ball, V. Bertone, S. Carrazza et al., "Parton distributions with LHC data", *Nucl.Phys.* **B867** (2013) 244–289, doi:10.1016/j.nuclphysb.2012.10.003, arXiv:1207.1303.

[37] H1 and ZEUS Collaboration, "HERAPDF1.5", *Proceedings of the 35th International Conference of High Energy Physics, Proceedings of Science* **168** (2010).

[38] S. Catani, L. Cieri, G. Ferrera et al., "Vector boson production at hadron colliders: A Fully exclusive QCD calculation at NNLO", *Phys.Rev.Lett.* **103** (2009) 082001, doi:10.1103/PhysRevLett.103.082001, arXiv:0903.2120.

[39] S. Catani and M. Grazzini, "An NNLO subtraction formalism in hadron collisions and its application to Higgs boson production at the LHC", *Phys.Rev.Lett.* **98** (2007) 222002, doi:10.1103/PhysRevLett.98.222002, arXiv:hep-ph/0703012.

[40] G. A. Ladinsky and C. P. Yuan, "The nonperturbative regime in QCD resummation for gauge boson production at hadron colliders", *Phys. Rev.* **D50** (1994) 4239, doi:10.1103/PhysRevD.50.R4239, arXiv:hep-ph/9311341.

[41] C. Balazs and C. P. Yuan, "Soft gluon effects on lepton pairs at hadron colliders", *Phys. Rev.* **D56** (1997) 5558–5583, doi:10.1103/PhysRevD.56.5558, arXiv:hep-ph/9704258.

[42] F. Landry, R. Brock, P. M. Nadolsky et al., "Tevatron Run-1 Z boson data and Collins-Soper-Sterman resummation formalism", *Phys. Rev.* **D67** (2003) 073016, doi:10.1103/PhysRevD.67.073016, arXiv:hep-ph/0212159.